Decadal Changes in Ventilation and Anthropogenic Carbon in the Nordic Seas

Emil Jeansson[1] , Toste Tanhua[2] , Are Olsen[3] , William M. Smethie Jr.[4] , Balamuralli Rajasakaren[1], Sólveig R. Ólafsdóttir[5] , and Jón Ólafsson[6]

[1]NORCE Norwegian Research Centre, Bjerknes Centre for Climate Research, Bergen, Norway, [2]GEOMAR Helmholtz Centre for Ocean Research Kiel, Kiel, Germany, [3]Geophysical Institute, University of Bergen and Bjerknes Centre for Climate Research, Bergen, Norway, [4]Lamont-Doherty Earth Observatory of Columbia University, Palisades, NY, USA, [5]Marine and Freshwater Research Institute, Hafnarfjordur, Iceland, [6]Institute of Earth Sciences, University of Iceland, Reykjavik, Iceland

Abstract We evaluate the decadal evolution of ventilation and anthropogenic carbon (C_{ant}) in the Nordic Seas between 1982 and the 2010s. Ventilation changes on decadal timescale are identified by evaluating decadal changes in mean ages and apparent oxygen utilization in each of the four main basins of the Nordic Seas (the Greenland and Iceland Seas, and the Norwegian and Lofoten Basins). The ages are derived from the transient time distribution approach, based on the transient tracers chlorofluorocarbon-12 (CFC-12) and sulfur hexafluoride (SF_6). The different decades show different phases in ventilation, with the 2000s being overall better ventilated than the 1990s in all basins. For the Greenland Sea, we also show that the 2010s are better ventilated than the 2000s, with a clear shift in hydrographic properties. The evolution of concentrations and inventory of C_{ant} is linked to the ventilation state. The deep waters get progressively older over the analyzed period, which is connected to the increased fraction of deep water from the Arctic Ocean.

Plain Language Summary The ocean region between Greenland, Iceland, and Norway, called the Nordic Seas, is a main site of deep-water formation. This process produces dense waters and brings surface waters to larger depths, thereby ventilating the water below. This transports, among other things, man-made CO_2 (anthropogenic carbon; C_{ant}) and oxygen from the atmosphere into the interior ocean, thereby reducing the amount of CO_2 stored in the atmosphere. This study investigates how the ventilation has changed in the Nordic Seas from 1982 to the 2010s. We find that the ventilation has changed with time, from a rather well-ventilated state in 1982, to a reduced ventilation in the 1990s, and then a restrengthened ventilation from the 2000s.

1. Introduction

Ocean ventilation is the process whereby surface water is transported into the ocean interior and interior water is transported back to the surface, sometimes in a different part of the world oceans and after long delay. This is important for ocean anthropogenic CO_2 (C_{ant}) sequestration (e.g., Fröb et al., 2016; Gruber et al., 2019; Khatiwala et al., 2013; Sabine & Tanhua, 2010; Sabine et al., 2004) and for the transport of other atmospheric gases such as oxygen, and heat as the surface waters that are transported to the interior ocean carry a signal of conditions in the atmosphere at the time of deep-water formation. The main sites for this process are found in the Southern Ocean and the North Atlantic (e.g., Khatiwala et al., 2013; Talley et al., 2011). In the sub-polar North Atlantic, strong vertical mixing occurs in the Labrador and Irminger Seas, and in the Nordic Seas (the collective term for the Greenland, Iceland, and Norwegian seas). The Nordic Seas is a very dynamic region and major site of water mass formation and transformation. This creates very dense waters that contribute to the North Atlantic deep water via the overflows across the Greenland-Scotland ridge (e.g., Chafik & Rossby, 2019; R. R. Dickson & Brown, 1994). In the so-called Arctic domain (e.g., Swift, 1986), consisting of the Greenland and Iceland Seas, open-ocean convection is frequent. In the Iceland Sea winter mixed layers are typically 200–300 m deep, and occasionally deeper than 400 m (Jeansson et al., 2015; Ólafsson, 2003; Våge et al., 2015). In the Greenland Sea, convection to depths between 1,000 and 1,600 m is common (e.g., Brakstad et al., 2019; Ronski & Budéus, 2005). Interannual variability in convection depth has been linked to changes in surface salinity in the Greenland Sea (Brakstad et al., 2019). Recently, an increase in oxygen content was reported for the Greenland Sea, attributed to a trend of deepening convection, and related to propagation of increasing salinity in the Atlantic waters that enter the Nordic Seas in the southeast (Lauvset et al., 2018). While changes in the Greenland Sea have been rather

well documented (e.g., Brakstad et al., 2019; Jeansson et al., 2017; Karstensen et al., 2005; Lauvset et al., 2018), changes in the ventilation in the other parts of the Nordic Seas over the past several decades are not well understood. From the observed spreading of intermediate water from the Greenland Sea to all other basins in the Nordic Seas (e.g., Jeansson et al., 2017; Messias et al., 2008) one would expect that at least the intermediate layers of the adjacent basins are affected by any change in the Greenland Sea.

In addition, it is important to understand the impact of changes in ventilation on the accumulation of C_{ant} in the region. Several studies have estimated Nordic Seas' C_{ant} inventories using different approaches. Based on relationships between nutrients, inorganic carbon, and the transient tracer CFC-11, Jutterström et al. (2008) estimated a Nordic Seas C_{ant} inventory of ∼1.2 Gt C in 2002. Similarly, Olsen et al. (2010), using the transit time distribution (TTD) approach (e.g., Hall et al., 2002; Waugh et al., 2006), calculated a C_{ant} inventory of 1.24 Gt C for the same year. The latter study found water column inventories of around 70 mol m^{-2} in the deep basins with stronger vertical mixing (i.e., the Greenland Sea and Lofoten Basin), but large horizontal gradients over the whole region. However, the temporal evolution of the inventory, and its drivers, remain to be evaluated. Using the extended multi-linear regression technique (Friis et al., 2005), Olsen et al. (2006) evaluated the change in C_{ant} in the Nordic Seas from 1981 to 2002/2003. They found the largest C_{ant} increases in the Atlantic domain, in the eastern part of the Nordic Seas (∼12–18 μmol kg^{-1}), while the deep waters showed a modest increase (4–6 μmol kg^{-1}).

The aim of this paper is to shed light on these questions for the four main basins of the Nordic Seas for the period from 1982 to 2016. To this end we utilize a combination of apparent oxygen utilization (AOU) and transient tracers, to evaluate decadal changes in ventilation as well as in the concentrations and water column inventories of C_{ant}.

1.1. Description of the Area, General Circulation, and Main Water Masses

The Nordic Seas are situated between the North Atlantic and the Arctic Ocean and are significantly affected by both. They are bounded by the relatively shallow Greenland–Scotland Ridge to the south, the shallow Barents Sea to the northeast, and the 2,600-m deep Fram Strait to the north. Several ridges and fracture zones divide the Nordic Seas into the four basins treated here (Figure 1).

The main circulation is cyclonic, with the northward flowing Norwegian Atlantic Current in the east, carrying warm and saline Atlantic Water, and the East Greenland Current (EGC) in the west carrying cold and relatively fresh Polar Surface Water southwards. The Norwegian Atlantic Current bifurcates several times in the northeastern Nordic Seas; some Atlantic Water enters the Barents Sea, some enters the Arctic Ocean through the eastern Fram Strait, and some re-circulates in the Fram Strait area and joins the EGC southward below the Polar Water. The Jan Mayen Current (Bourke et al., 1992) branches off the EGC eastward in the southwestern Greenland Sea and the East Icelandic Current branches off eastward in the Iceland Sea. Both currents inject cold and relatively fresh water masses from the EGC to the central parts of the Nordic Seas; for example, the East Icelandic Current continues all the way to the southern Norwegian Sea (Macrander et al., 2014; Swift & Aagaard, 1981). Warmer and saltier waters also enter the Norwegian Sea interior with westward moving branches of the Norwegian Atlantic Current, particularly those associated with the Vøring Plateau and Fram Strait (Poulain et al., 1996).

In addition to the Atlantic Water and Polar Water, different water masses are formed in the region. The open-ocean convection in the Greenland Sea forms the Greenland Sea Arctic Intermediate Water (GSAIW), while the much shallower convection in the Iceland Sea forms Iceland Sea AIW (e.g., Jeansson et al., 2017). These spread around the Nordic Seas, contributing to the Norwegian Sea AIW (e.g., Blindheim, 1990; Jeansson et al., 2017), and are incorporated into the dense overflows (e.g., Jeansson et al., 2008; Olsson et al., 2005; Tanhua, Olsson, & Jeansson, 2005). The deep layers of the Greenland Sea consist of two types of deep waters: an upper layer dominated by dense water from the Arctic Ocean that enter the region through the Fram Strait—here referred to as Greenland Sea Deep Water (GSDW)—and deep water formed locally in the Greenland Sea—here referred to as Greenland Sea Bottom Water (GSBW) (e.g., Rudels et al., 1999, 2005). The deep waters in the Iceland and Norwegian Seas are a mixture of these waters (e.g., Blindheim & Rey, 2004).

2. Data and Methods

2.1. Data

The data used in the present study have been extracted from the 2019 update of the Global Ocean Data Analysis Project version 2 data product (GLODAPv2.2019), which has been subjected to rigorous quality control as
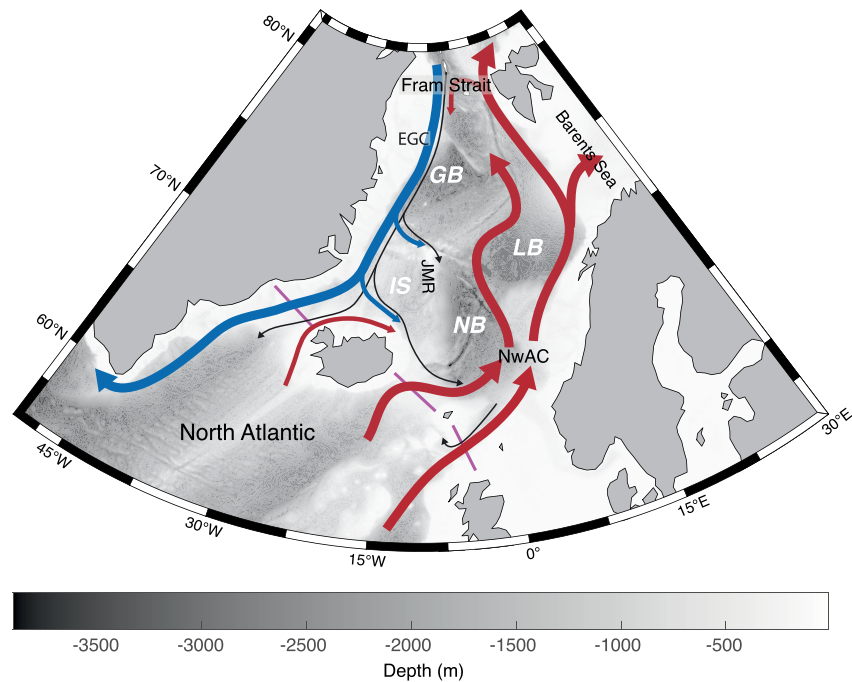
Figure 1. Map of the Nordic Seas showing bathymetry from ETOPO1, currents, and geographical features. The warm surface currents of Atlantic Water are depicted in red, and cold fresher surface currents from the Arctic Ocean are shown in blue. The thin black lines indicate the flow of denser waters. The magenta lines show the Greenland–Scotland Ridge (from west to east: Denmark Strait, Iceland–Faroes gap and Faroe–Shetland Channel). Abbreviations: EGC, East Greenland Current; GB, Greenland Basin; IS, Iceland Sea; JMR, Jan Mayen Ridge; LB, Lofoten Basin; NB, Norwegian Basin; NwAC, Norwegian Atlantic Current.

described in Olsen et al. (2019). The variables used are potential temperature, salinity, dissolved oxygen, and the transient tracers chlorofluorocarbon-12 (CFC-12) and sulfur hexafluoride (SF_6). The reason to use GLODAP data is the transient tracers and oxygen data, at high accuracy. The accuracy of the GLODAPv2.2019 data product is reported to be better than 0.005 in salinity, 1% in oxygen, and 5% in CFC-12 (Olsen et al., 2019). SF_6 quality control was only introduced in GLODAPv2.2022 (Lauvset et al., 2022). This indicated that the SF_6 data used here (from 2016) were unbiased. The precision of these 2016 SF_6 data was assessed at the cruise in question, by collecting and analyzing multiple water samples from the same depth at a single CTD-cast, at ~1.7%. Furthermore, for the Iceland Sea, we include previously unpublished CFC-12 data sampled between 2002 and 2006 in a cooperative project between the Marine Research Institute in Reykjavik and the Lamont-Doherty Earth Observatory (LDEO). These tracer data are not part of GLODAPv2.2019, but available as a separate data set (Ólafsson et al., 2023). Concurrent oxygen and other data from these Iceland Sea cruises are already included in GLODAPv2.2019. The samples were collected in glass ampoules, flame sealed under nitrogen flow and later analyzed at the LDEO. These CFC-12 data have a precision of ~1%, or 0.01 pmol kg^{-1}, whichever is greater.

We utilized data from 1982 to 2016 (when available) from each of the four main basins: the Greenland Sea (represented by the Greenland Basin), the central Iceland Sea, and the two basins of the Norwegian Sea (Norwegian Basin and Lofoten Basin), with the "iconic" Hudson cruise in 1982 (Bullister & Weiss, 1983) as a starting reference. Data were extracted from within the four circles shown in Figure 2, positioned in the center of each basin to reduce any effects from slopes and boundary currents (see Figure 2 caption for the exact definition of each of these circles).

The tracer concentrations are presented as partial pressure (pCFC-12 and pSF_6 in pico (10^{-12}) atmospheres or parts per trillion, ppt). The pCFC (or pSF_6) of a water sample is computed based on the expression pCFC (or pSF_6) = $C_{SW}/F(\Theta, S)$ (Doney & Bullister, 1992), where C_{SW} is the concentration (in pmol kg^{-1}, for CFC-12, and fmol kg^{-1}, for SF_6) of the dissolved tracer in the seawater sample and $F(\Theta, S)$ is the solubility of the tracer (in mol kg^{-1} atm^{-1}), determined from potential temperature and salinity (Bullister et al., 2002; Warner & Weiss, 1985).
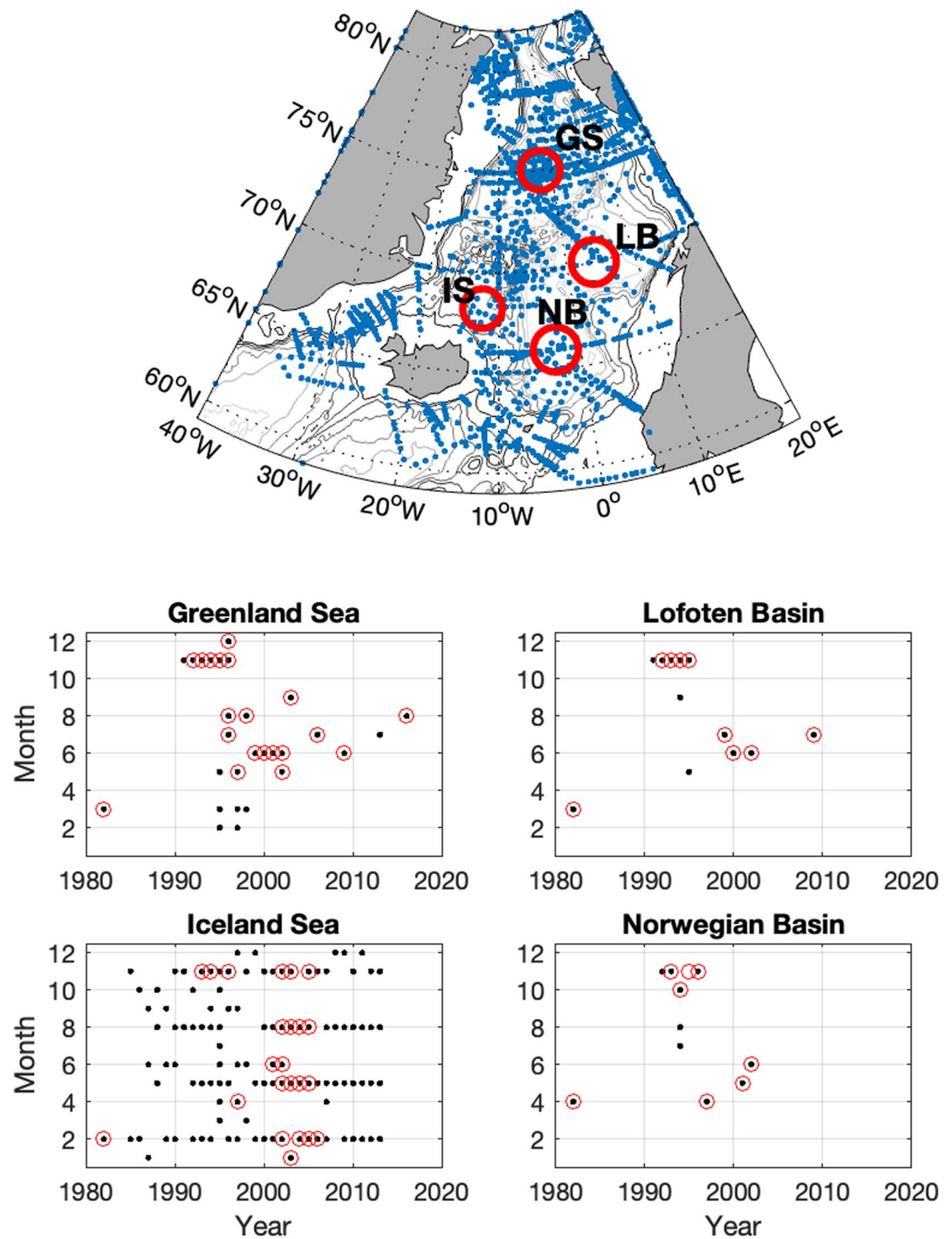
Figure 2. (upper) Map showing the data distribution and geographic definitions used for the different basin properties (circles). GS, Greenland Sea; IS, Iceland Sea; LB, Lofoten Basin; NB, Norwegian Basin. The isobaths mark every 500 m. The circle coordinates and radii are as follows: Greenland Sea: 75°N, −2°E, 110 km; Iceland Sea: 68°N, −12°E, 110 km; Norwegian Basin: 66°N, −3°E, 125 km; Lofoten Basin: 70°N, 4°E, 125 km. The four lower panels show the data distribution in each of the four basins over the analyzed period. Black dots mark available oxygen data, and red circles mark available CFC-12 data, from the surface to the bottom.

CFC-12 and SF_6 enter the surface ocean via air–sea exchange, based on the solubility functions referenced above, and are propagated into the interior with the ocean circulation and mixing. The air–sea equilibrium timescale for the surface mixed layer is approximately 1 month (Gammon et al., 1982), hence the ocean surface concentrations tend to track, and can be estimated from, the atmospheric history. Because CFC-12 and SF_6 are inert in
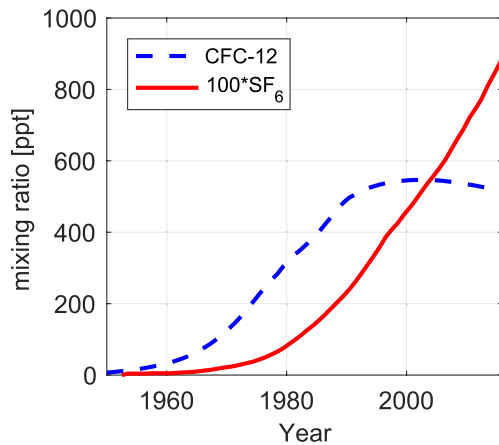
Figure 3. Atmospheric histories of CFC-12 and SF$_6$ between 1950 and 2016 in the northern hemisphere (Bullister, 2015; Walker et al., 2000). Note that the SF$_6$ values are multiplied with 100 for easier comparison.

seawater, an increase of their concentration is an unequivocal sign of ventilation, although the recent atmospheric evolution makes it impossible to use CFC-12 to assess unique ventilation ages for recently formed water masses (Figure 3). SF$_6$ is still increasing in the atmosphere and is thus useful to assess the ventilation history of more recently formed waters (e.g., Sonnerup et al., 2008; Tanhua et al., 2008).

The surface concentration of AOU is independent of temperature and salinity and does not change with time, except seasonally due to biological activity. Thus, a decrease in AOU in the ocean interior (i.e., an increase in oxygen) is a sign of ventilation. AOU is calculated as the difference between the saturation concentration, and the measured concentration of oxygen. AOU is possibly a more robust tracer for evaluating ventilation changes than CFC or SF$_6$ derived water mass ages (A. E. Shao et al., 2016), assuming no change in respiration. Here, AOU and water mass ages are used in combination. It is important to be aware that at constant ventilation both AOU and mean age would be expected to be more or less constant, but there would be an increase in C$_{ant}$ due to the atmospheric increase. Similar directions of change in both AOU and mean age is a very firm indicator of changing ventilation. Nevertheless, a strong relationship between AOU and mean age does not always apply (e.g., Koeve & Kähler, 2016; J. L. Thomas et al., 2020). This is further discussed in Section 4.2.

2.2. Transit Time Distribution Approach

To assess the age and associated concentration of C$_{ant}$ of the various water masses in the Nordic Seas we use the TTD approach (e.g., Hall et al., 2002; Waugh et al., 2004, 2006). The method is based on measurements of transient tracers, such as the CFCs and SF$_6$, infers the age distribution of a water sample, and uses this age distribution and solubility considerations to estimate the concentration of C$_{ant}$. The concentration of any passive tracer, $c(r, t)$, at a point r is related to its surface water history $c_0(t)$ by the function:

$$c(r, t) = \int_0^\infty c_0(t - t') G(r, t') dt',$$

(1)

where $G(r, t')$ is the TTD at point r (e.g., Haine & Hall, 2002). The input function of the tracers at the sea surface, $c_0(t)$, is determined from the atmospheric history of the tracers and their solubilities. Here, we have used the atmospheric history of CFC-12 from Walker et al. (2000), updated with values from Bullister (2015), and the atmospheric history of SF$_6$ from Bullister (2015).

It is assumed that the TTDs can be approximated by an inverse Gaussian function:

$$G(t) = \sqrt{\frac{\Gamma^3}{4\pi\Delta^2 t^3}} \exp\left(\frac{-\Gamma(t - \Gamma)^2}{4\Delta^2 t}\right),$$

(2)

where the extent of mixing is represented by the ratio of the width of the TTD (Δ) to the mean transit time ("mean age"; Γ). With this assumption together with the assumption of a constant Δ/Γ ratio, the mean age can be found from the tracer concentration (and T and S) (Waugh et al., 2004, 2006). A Δ/Γ of 0 represents a purely advective flow, $\Delta/\Gamma < 1$ indicates a predominantly advective flow, and for $\Delta/\Gamma > 1$ diffusive processes dominate the mixing and circulation. The Δ/Γ ratio can be constrained by two tracers with different atmospheric time histories (e.g., Waugh et al., 2003, 2004). A common pair is CFC-12 and SF$_6$ (e.g., Stöven et al., 2016; Tanhua et al., 2008). However, SF$_6$ is problematic in the Nordic Seas due to the deliberate release and subsequent spreading of large amounts (320 kg) of this tracer in the Greenland Sea in 1996 (Jeansson et al., 2009; Marnela et al., 2008; Messias et al., 2008; Tanhua, Bulsiewicz, & Rhein, 2005; Watson et al., 1999). This excess SF$_6$ may have affected the transient signal even as late as 2012, in the Fram Strait (Stöven et al., 2016). Therefore, we used CFC-12 for most years in the present study, except for 2016 in the Greenland Sea (where SF$_6$ was used for the upper 1,800 m). We have further adopted a Δ/Γ ratio of 1, which has been found to best describe the data in the Nordic Seas (Olsen

et al., 2010) and is also commonly applied elsewhere (e.g., Tanhua et al., 2008; Waugh et al., 2004, 2006). This implies rather strong mixing, resulting in wide age spectra, and hence the uncertainty in the age estimates is relatively large, especially at higher ages (see, e.g., Stöven et al., 2015). Based on a model evaluation He et al. (2018) suggested that a ratio of 0.8 may be more appropriate than unity. Nevertheless, since we could not test the validity of this with the data at hand, we adopted the more common unity ratio. Thus, we may have overestimated the mean age, particularly for the deep waters. Rajasakaren et al. (2019) constrained the Δ/Γ ratio in the Arctic Ocean and suggested different ratios for upper and deeper waters; as low as 0.6 in the upper and intermediate waters and 1.2 at greater depths, as well as regional differences. This may also be the case in the Nordic Seas, and future evaluations might shed more light on this, when the signal of excess SF_6 from the release is washed out further. However, in a very recent study Smith et al. (2022) found support for a Δ/Γ ratio of about 1 in the Arctic Ocean. Measurements of additional tracers could be useful to better constrain the shape of the TTD, which may also have a different shape than an inverse Gaussian (see e.g., work from the Mediterranean Sea; Stöven & Tanhua, 2014). The combination CFC-12 and Argon-39 has been shown to provide powerful constraints on Δ/Γ ratios (e.g., Ebser et al., 2018).

The surface saturation of the tracer in question can also impact the TTD calculations, as the combination of atmospheric concentration and saturation defines the input function. It is often assumed that the surface waters have a constant saturation (100% or less) at the time of descent, which for many regions is a fair assumption (e.g., Fine et al., 2017). However, in parts of the Nordic Seas and other regions with active and strong winter convection, that is, deep winter mixed layer, the surface waters are typically undersaturated in winter, which is the time they descend to greater depths (e.g., Anderson et al., 2000; Bullister & Weiss, 1983; Rhein, 1991; Wallace & Lazier, 1988). This is particularly true during the time the atmospheric concentration of the tracer is rapidly increasing, between 1960s and the 1990s (Figure 3). Observational data from these regions are typically biased toward summer, when the surface waters are warmer, and then also closer to full saturation (e.g., Jeansson et al., 2010; A. E. Shao et al., 2013). This is also true for the data included in the present analysis, where all four basins show a surface saturation (upper 20 m) between 97% and 100% (not shown). To determine more realistic values for winter surface saturation levels we instead chose the 100–200 m layer, since this layer was shown to be more stable in both tracer saturation and temperature (Figure S1 in Supporting Information S1). This reduced the mean saturation for CFC-12 from 97% to 78% in the Greenland Sea, from 98% to 87% in the Iceland Sea, from 99% to 92% in the Norwegian Basin, and from 100% to 97% in the Lofoten Basin. However, the CFC-12 saturation is not constant and seems to increase with time (Figure S2 in Supporting Information S1). This is in agreement with what has been found in the North Atlantic (Tanhua et al., 2008) and the Labrador Sea (Raimondi et al., 2021). This evolution is most clearly seen in the Greenland Sea, but also seems to be the case in the other basins. Details of the procedure are found in Supporting Information S1.

For SF_6, a constant saturation state was used for all basins, due to the excess SF_6 it is not possible to evaluate time trends. This was taken as the mean saturation in the 100–200 db layer, 79% in the Greenland Sea, and 100% in the other basins (see Figure S1 in Supporting Information S1).

With knowledge of the TTD ($G(t)$), and assuming that C_{ant} propagates into the ocean interior as a passive tracer, Equation 1 can be used to calculate concentrations of C_{ant} at any location (Hall et al., 2002; Waugh et al., 2004, 2006), which also requires a surface history of C_{ant}. This is calculated from equilibrium inorganic carbon chemistry, as the difference in saturation concentrations of dissolved inorganic carbon (DIC) concentrations between any time t and pre-industrial times, $C_{ant,0}(t) = C_{eq}(T, S, Alk^0, pCO_2(t)) - C_{eq}(T, S, Alk^0, pCO_2 = 280)$, where C_{eq} is the DIC, T the temperature, S the salinity, Alk^0 the preformed alkalinity and $pCO_2(t)$ the atmospheric partial pressure of CO_2 at time t; 280 ppm is used as the pre-industrial atmospheric pCO_2. C_{eq} is calculated using the seawater CO_2 chemistry equilibria, with the preformed alkalinity estimated from the surface salinity to alkalinity relationship determined for the Nordic Seas by Nondal et al. (2009), and the equilibrium constants of Merbach et al. (1973), refit by A. G. Dickson and Millero (1987). Atmospheric CO_2 concentrations were extracted from the Mauna Loa record (Tans and Keeling, available at https://www.esrl.noaa.gov/gmd/ccgg/trends/data.html).

2.3. Mean Profiles and Inventory Calculations

Annual average profiles for each basin were constructed. This was done by first calculating annual mean values for pre-defined depth layers: every 50 m in the upper 200 m, every 100 m down to 2,000 m, and every 250 m from 2,000 m down to the bottom. To fill in missing values each of these mean profiles were interpolated via

piecewise cubic Hermite interpolation (Fritsch & Carlson, 1980) because this method is not prone to "ringing." From these annual means we then calculated decadal means of AOU, mean age and C_{ant} for the depth layers: 200–500, 500–1,000, 1,000–1,500, 1,500–2,000, 2,000–3,000, and, 3,000–4,000 m in each of the four basins. For the shallower Iceland Sea only depths down to 2,000 m were considered.

Column inventories of C_{ant} in 1982, 1990s, 2000s, and 2010s (the latter only for the Greenland Sea) were calculated for each basin, by multiplying the mean concentration of C_{ant} (in µmol kg^{-1}) in each layer with the mean density (in kg m^{-3}) and thickness of the layer (in meters), down to the bottom of each basin. The bottom depths were estimated from the mean bottom depth in each basin. The resulting depths were 3,589 m for the Greenland Sea, 1,879 m for the Iceland Sea, 3,381 m for the Norwegian Basin, and 3,178 m for the Lofoten Basin. Summing up all layers for each period gives the column inventory (in mol m^{-2}). Using mean bottom depths will exclude any depths below the mean depth, which will introduce a bias. However, the main aim is here to look at changes in inventories as a result of ventilation changes. As such the bottom depths will have a limited impact on the results.

2.4. Uncertainties

There are uncertainties related to the different assumptions in the TTD approach, but also in the assumptions made when calculating AOU values. For the TTD approach the main uncertainties are related to the surface saturations of the tracers, the assumed mixing (Δ/Γ), and the assumption of a constant disequilibrium of CO_2 for the calculation of C_{ant} from the mean age (e.g., He et al., 2018; Waugh et al., 2006). For AOU the main uncertainty is connected to the assumption that the sea surface is in full equilibrium with the atmosphere. This is not always the case, as has been shown for the Nordic Seas (e.g., Olsen et al., 2010), or the Labrador Sea (Atamanchuck et al., 2020). Below we will quantify the sensitivity of our calculations to the applied assumptions.

To evaluate the sensitivity of the calculated decadal means to the different assumptions for the TTD approach we performed the calculations with different mixing scenarios (Δ/Γ), and different surface saturations of CFC-12.

The Δ/Γ ratio has a clear impact on the mean ages, especially below 1,500 m (Figure 4). Compared to our applied ratio of 1, a lower ratio (0.8) results in 21%–26% lower ages below 1,500 m, while a higher ratio (1.2) give 26%–31% higher ages. For C_{ant}, the impact of Δ/Γ was much lower than for the mean age. The lower Δ/Γ (0.8) gave between 4% and 7% higher concentrations below 2,000 m, and mostly within 3% higher at shallower depths (Figure 4). A higher Δ/Γ (1.2) resulted in 3%–5% lower concentrations below 2,000 m, and within 3% higher up in the water column. The difference in uncertainty between age and C_{ant} is a consequence of the atmospheric growth rate of C_{ant}. When the old deep waters were formed the growth rate was low, so the large impact of changes in age does not have a corresponding impact on C_{ant}. For more recently ventilated waters the uncertainty in age is relatively low, leading to small uncertainties in C_{ant} despite the recent high growth rate in the atmosphere. An additional source of uncertainty is that we assume that the Δ/Γ ratio does not change over time. This is, however, not possible to explore with the tracers we use.

The applied surface saturation has a much smaller impact on both ages and C_{ant} (not shown) that is well within the decadal uncertainty. Nevertheless, the constant saturations resulted in slightly higher ages compared to the time-dependent saturation, with the largest deviation of up to 17% higher, which is much higher than the analytical error of the tracers. These results agree well with what He et al. (2018) found in their evaluation.

The uncertainty in the calculated AOU values, taken from the GLODAPv2.2019 data product, is connected to the assumption that the surface water was in full equilibrium with the atmosphere at the time of descent. This assumption has been shown to be flawed in certain regions, and seasons (e.g., Ito et al., 2004; Koeve & Kähler, 2016). As seen in Supporting Information S1 (Figure S5) the assumption of 100% saturation in the surface layer (here taken as the upper 20 m) does not hold for any of the analyzed basins. Supersaturation of oxygen is expected during Spring/Summer due to biological production. The seasonal timing of the cruises toward the summer months (see Figure 2) could partly explain the trend of increasing saturations with time in the Greenland and the Norwegian Seas. In the Iceland Sea, the data show large seasonal variability, and for summer (high values) there is a trend of increasing saturations until the early 1990s, then stable and high saturations close to 110% during the 1990s and decreasing values after the mid-2000s. Nevertheless, with the same argumentation as for the tracers, since there is a general summer bias in the data product a more representative winter value is found below the top surface.

We tested this hypothesis for both AOU and CFC-12 by taking advantage of the Iceland Sea data, which have much better seasonal coverage than the other basins, by comparing the properties in the surface and the 100–200 m layer (Figure S6 in Supporting Information S1). The deepest mixed layer in the Iceland Sea is typically found in March (e.g., Jeansson et al., 2015; Våge et al., 2015). Unfortunately, we lack tracer data for March in this basin.
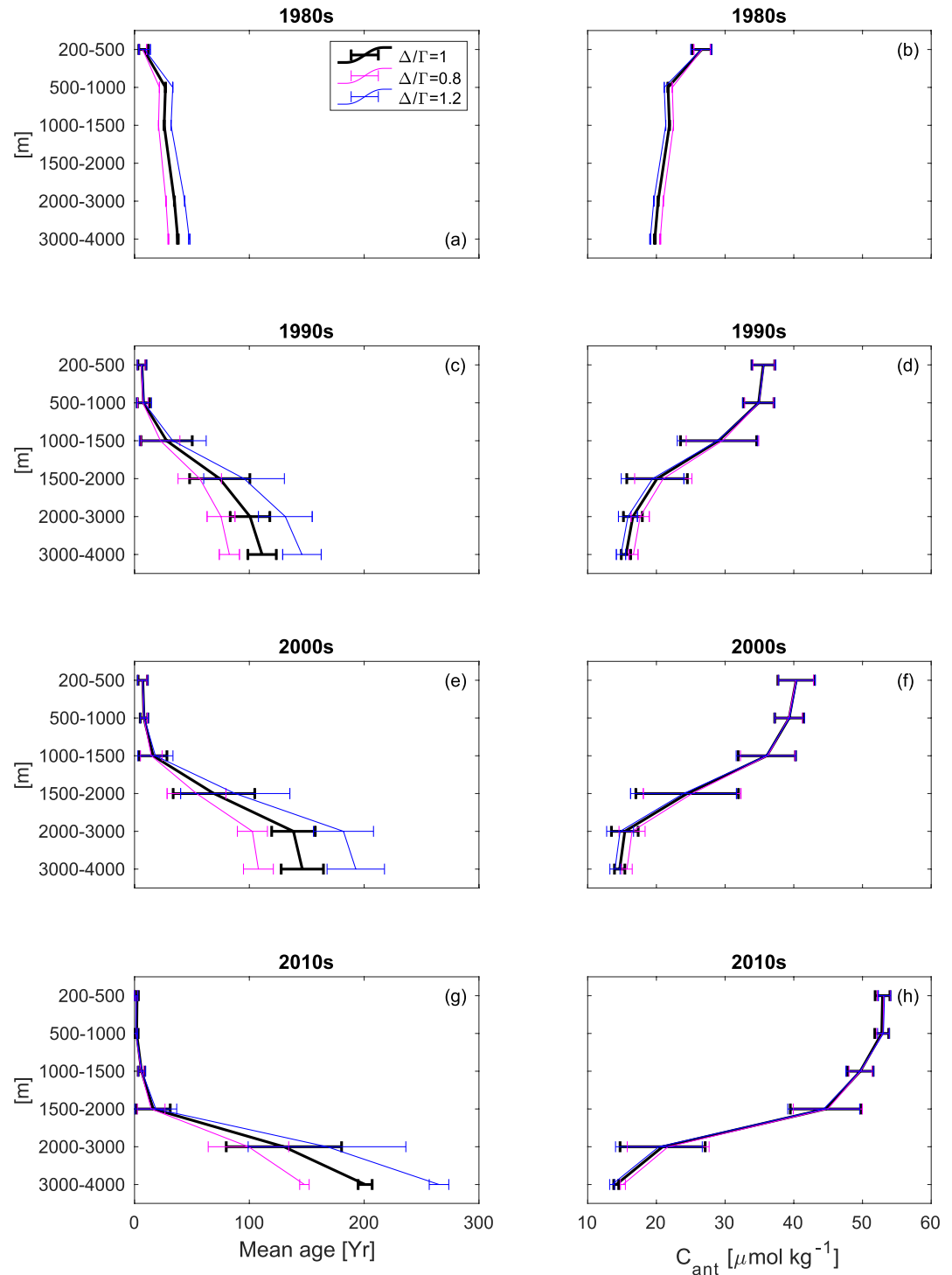
Figure 4. Uncertainty in decadal means (one row per decade) in mean age (a, c, e, g) and C_{ant} (b, d, f, h) in the Greenland Sea from different Δ/Γ (0.8–1.2). The error bars show the standard deviations of the decadal means.

For the available winter months, the CFC-12 saturation is somewhat lower in the sub-surface layer than in the surface, but within a reasonable agreement considering the uncertainties. For oxygen saturation, temperature, and salinity, however, the sub-surface layer indeed corresponds very well to the winter surface. In all basins, the oxygen is slightly undersaturated in the 100–200 m layer, and more or less constant with time. Since we in this work evaluate the changes over time to identify ventilation changes, we argue that the deviation from full

saturation does not affect our results. If, however, the AOU values are used to quantify respiration, this needs to be accounted for.

The last source of uncertainty we will discuss here is the potential impact of changes in the surface CO_2 saturation, often referred to as the air-sea CO_2 disequilibrium, on our results. This will have an impact on the calculated C_{ant} concentrations. Changes in the disequilibrium have been found to translate almost linearly to the C_{ant} values both in the Nordic Seas and the Labrador Sea (Olsen et al., 2010; Raimondi et al., 2021). Consequently, an ocean surface with a $p CO_2$ growth rate of 80% compared to the atmospheric $p CO_2$, will reduce the C_{ant} estimates by 20%.

3. Results

3.1. Distribution of Mean Age and C_{ant} in the Nordic Seas

Before evaluating any changes, we provide an example of the distribution of mean ages and C_{ant} at five depth layers in the upper 3,000 m of the Nordic Seas by using data for the year 2002, which covered most parts of the Nordic Seas (e.g., Jutterström et al., 2008; Olsen et al., 2010). For these figures we applied the Greenland Sea CFC-12 source function on all data with a density anomaly more than 27.9 kg m^{-3} and the Norwegian Sea CFC-12 source function for all data at lower densities. Our targeted layers are the mean depths of the upper five layers analyzed in this study, that is, 350, 750, 1,250, 1,750, and 2,500 m.

The age distribution reflects the different domains and the general circulation of the region (Figure 5). At 350 m, most of the Nordic Seas waters are less than 10 years old. The exception is the Iceland Sea, which here show ages of 10–20 years. At 750 m there is a clearer gradient, where the Lofoten Basin and the Greenland Sea show ages less than 10 years. The lower age in the Lofoten Basin is connected to the wider and deeper distribution of recently ventilated Atlantic Water, while this layer in the Greenland Basins is the core for the recently ventilated GSAIW. In contrast, in the south/southwestern parts of the area water mass ages are in the range of ~20–40 years. These older ages reflect the water masses that have circulated around parts of the Arctic Ocean and are carried by the East Greenland Current to these parts of the Nordic Seas. At 1,250 m the youngest waters, of about 10–20 years, are found in the Greenland Sea, a consequence of the deep winter mixed layers. Similar ages are encountered at these depths in the Lofoten Basin. This is below the Atlantic Water (Figures S7 and S8 in Supporting Information S1) and associated with GSAIW spreading from the Greenland Sea (e.g., Jeansson et al., 2017). This is also supported by the distribution of AOU (Figure S10 in Supporting Information S1). The less ventilated southern parts of the region, the Iceland Sea and Norwegian Basin, show ages of 60–80 years at these depths. At 1,750 m the ages are greater than at 1,250 m, but the spatial pattern is similar. The ages in the Greenland Sea and Lofoten Basin are in the range of 60–80 years. Elsewhere, water mass ages are 130–140 years at these depths. The ages in the deep water (2,500 m) have similar gradients; in the deep Greenland Sea ages are 140–150 years, while the in the deep Norwegian Sea ages are 160–170 years.

The distribution of C_{ant} is almost the inverse of the age distribution, following the overturning in the Nordic Seas (Figure 6), but somewhat modified by the fact that warm and salty waters (e.g., Atlantic Water) take up more C_{ant} than cold and fresh water (e.g., AIW). At 350 m, the highest concentrations are found in the Atlantic Water in the east (45–50 μmol kg^{-1}). The higher temperature, and thus buffer capacity, of the Atlantic Water allows for more uptake of C_{ant}, which is in contrast to uptake of gases that is higher at lower temperatures and lower salinities (e.g., Maier-Reimer & Hasselmann, 1987; H. Thomas & England, 2002). This is clearly illustrated by the gradient in C_{ant} from the east to the west, where the colder western parts of the Nordic Seas has the lowest concentrations of C_{ant} at these depths (~35–40 μmol kg^{-1}). At 750 m, the highest concentrations are found in the Lofoten Basin (~40 μmol kg^{-1}), as a result of the deeper extent of Atlantic Water there (e.g., Nilsen & Falck, 2006). The concentration in the central Greenland Sea is also relatively high. The concentrations in the southwestern regions are much lower (~25–30 μmol kg^{-1}), a consequence of the greater age and lower temperatures in this region. At the 1,250 m level, the central Lofoten Basin and the Greenland Sea show the highest concentrations, of ~30–35 μmol kg^{-1}. The south/southwestern parts of the region have concentrations of ≤25 μmol kg^{-1}. At 1,750 m the Greenland Sea and the Lofoten Basin still show the highest concentrations, of >20 μmol kg^{-1}, while the southern parts of the area have concentrations of about 15 μmol kg^{-1}. The deep waters (2,500 m) all have concentrations of ≤15 μmol kg^{-1}.

3.2. Decadal Changes in Hydrography, Mean Age, AOU, and C_{ant}

In this section we describe the decadal changes in hydrography (Θ/S), AOU, mean age and concentrations of C_{ant}, in the four main basins. Six depth layers are evaluated, below 200 m (see Section 2.3).
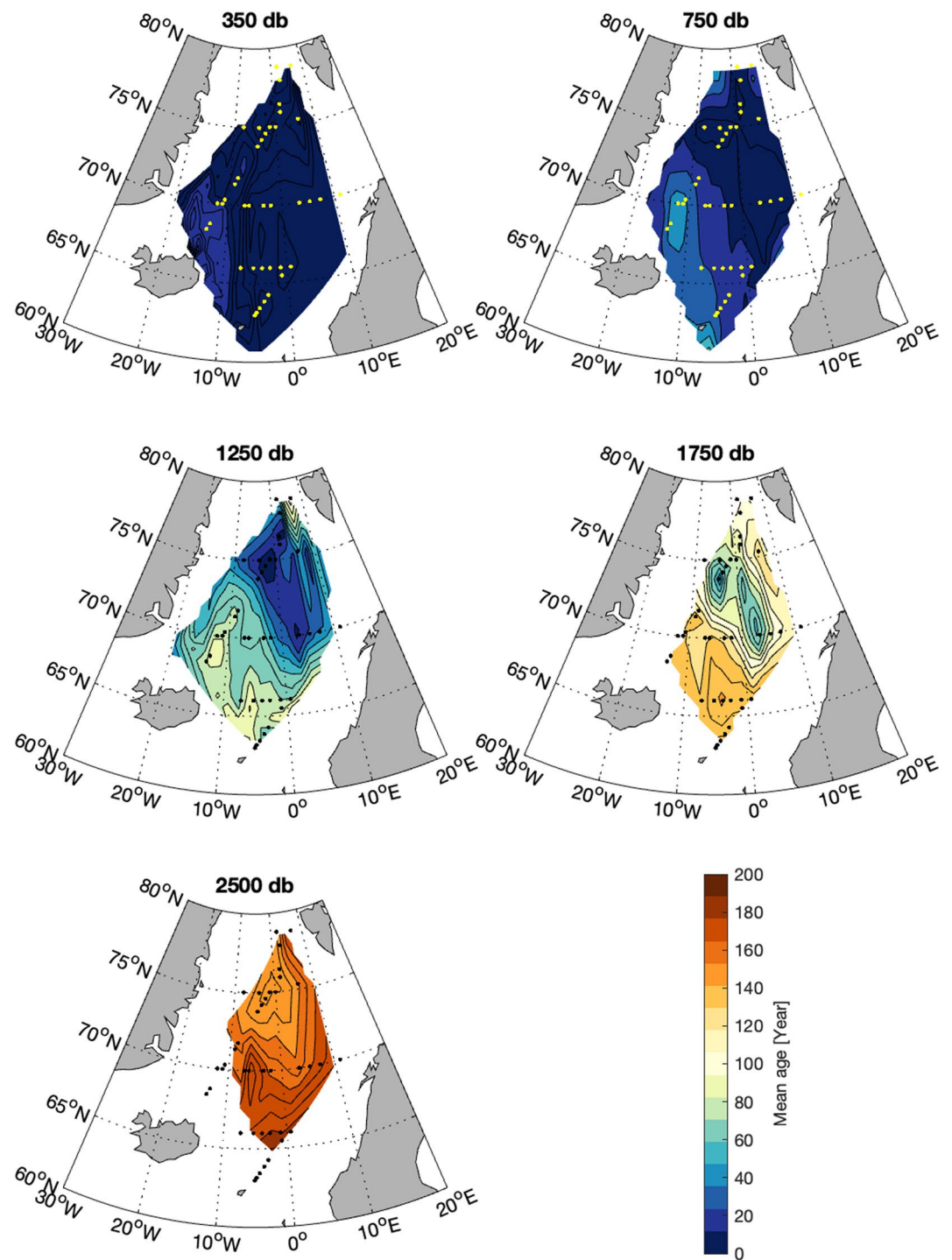
Figure 5. Distribution of mean age (from TTD using CFC-12) at different depth layers in the Nordic Seas in 2002; 350 db (upper left), 750 db (upper right), 1,250 db (middle left), 1,750 db (middle right), and 2,500 db (lower left).

3.2.1. Greenland Sea

There has been striking warming in all layers of the Greenland Sea over the analyzed period, and the largest warming, ~1°C from 1982 to the 2010s, took place in the upper layer (Figure 7). In 1982 the temperature was well below −1°C at all depths, while there was a clear gradient in the 2010s. For the 200–500 m layer, the warming was fastest (0.5°C per decade) between 1982 and the 1990s, and between the 2000s and the 2020s, while the
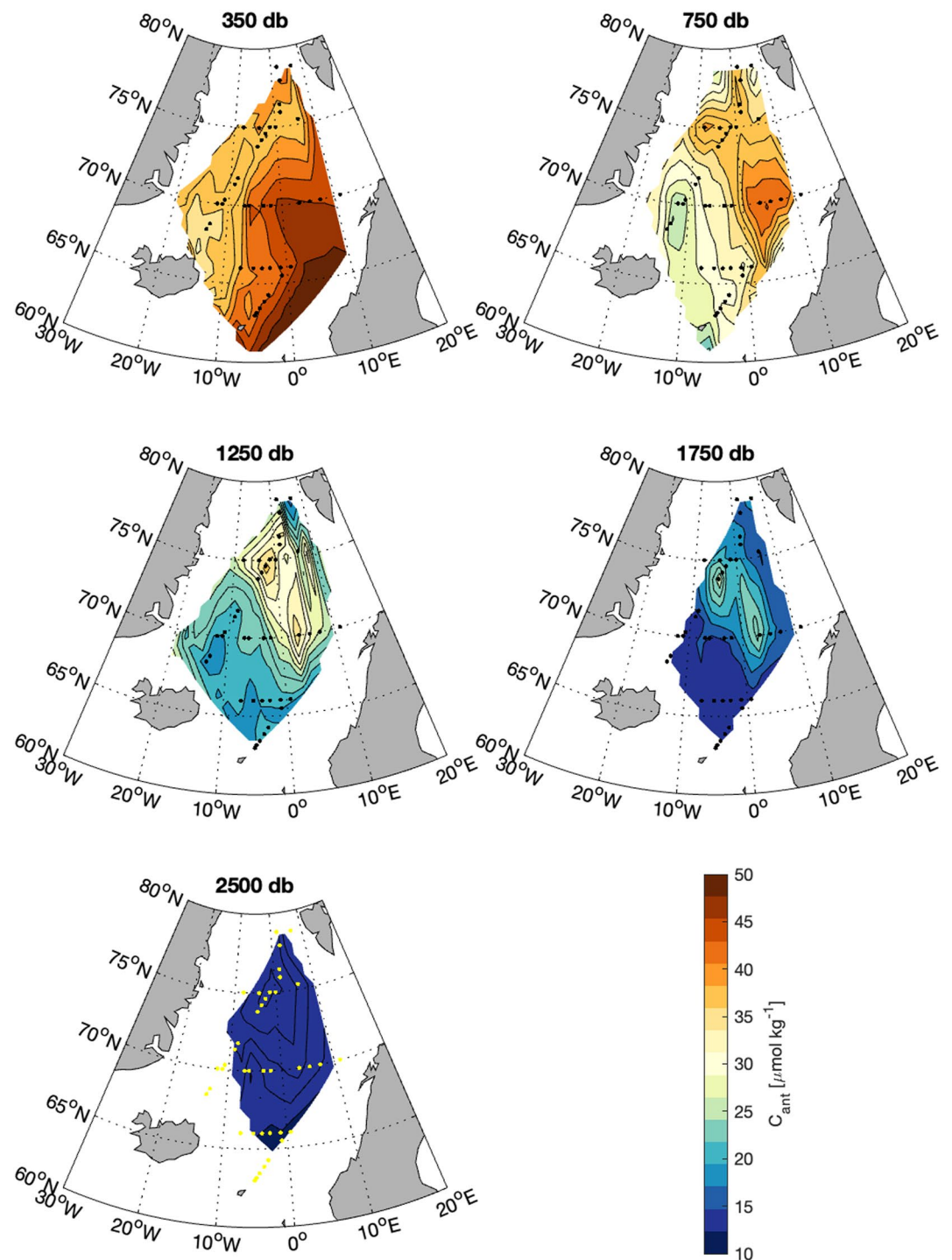
Figure 6. Distribution of C_{ant} (from TTD using CFC-12) at different depth layers in the Nordic Seas in 2002; 350 db (upper left), 750 db (upper right), 1,250 db (middle left), 1,750 db (middle right), and 2,500 db (lower left).

change from the 1990s to the 2000s was modest (0.1°C). For the layers between 500 and 1,500 m, the warming was the fastest between the 2000s and the 2010s (almost 0.4°C). There were also clear changes in salinity over the decades. In 1982 all depths had a salinity below 34.9, while the 2010 salinities were all between 34.91 and 34.92. The salinity increase in the upper part of the water column is connected to the higher salinity of the Atlantic Water entering the Nordic Seas (e.g., Holliday et al., 2008), and the increase in the deep waters is due to the increased
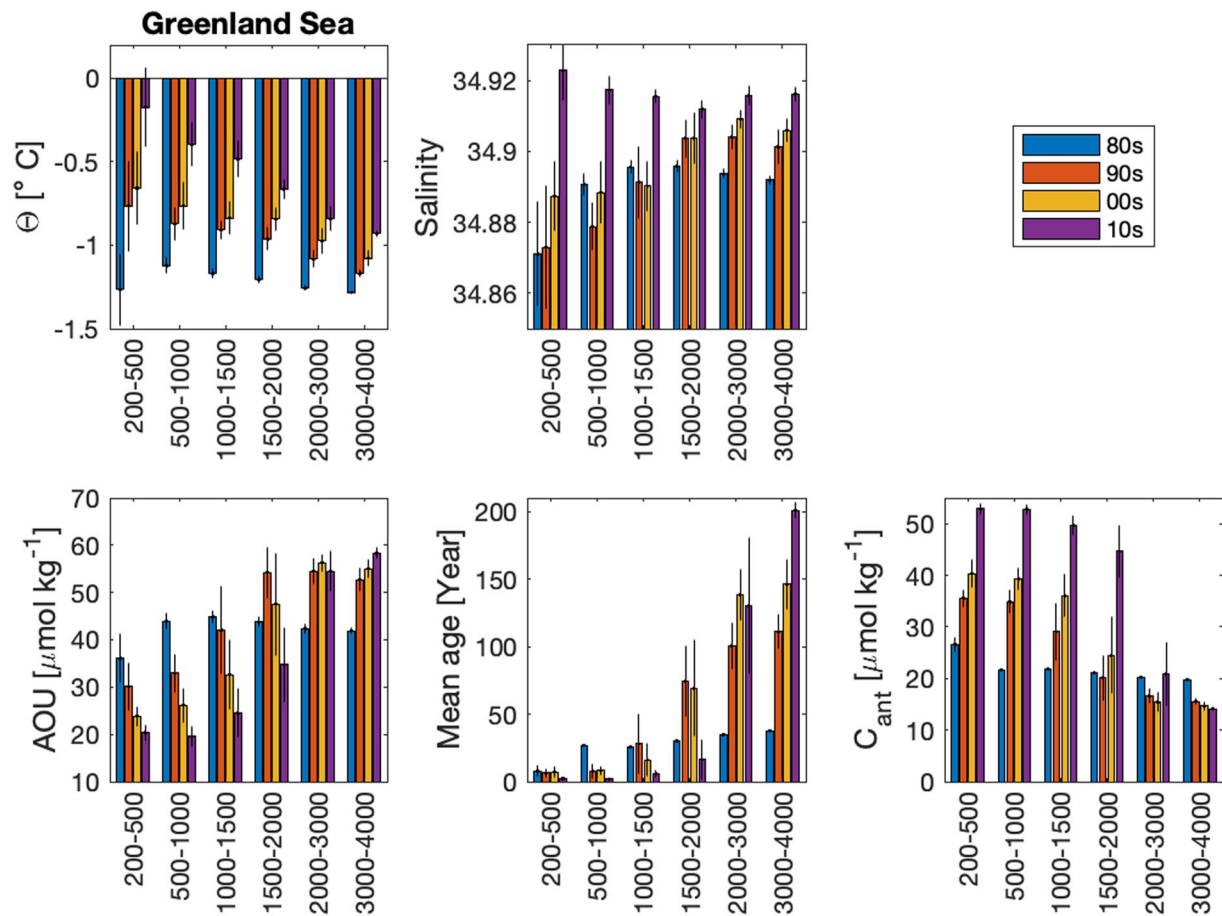
Figure 7. Decadal changes (comparing 1982, the 1990s, the 2000s, and the 2010s) in potential temperature, salinity, AOU, mean age and C_{ant} for different depth layers in the Greenland Sea. The colors indicate the different decades. The error bars indicate the standard deviations of the decadal means for each layer.

fraction of Arctic Ocean deep water (e.g., Somavilla et al., 2013). The salinity increase in the upper layer between the 2000s and the 2010s (0.035) was the fastest observed over the analyzed period, and more than twice the rate observed between the 1990s and the 2000s. Also for the depths between 500 and 1,500 m the increase from the 2000s to the 2010s was the greatest observed during the evaluated period.

All layers above 1,500 m show declining mean AOU with time, reflecting increased ventilation. The 1,500–2,000 m layer does not show any specific trend, but instead large variations in AOU, which can be linked to variations in convection; this first weakened from the 1980s to the 1990s, and then strengthened again in the 2000s and the 2010s.

In the deep water (below 2,000 m) the clearest change in AOU is the significant increase from the 1980s to the more recent decades (Figure 7 and Table 1). There is a small difference in the development of the GSDW (2,000–3,000 m) and GSBW (below 3,000 m), with GSDW being stable from the 1990s to the 2010s, while GSBW showed a small increasing trend in AOU, reflecting the increased intrusion of deep waters from the Arctic Ocean.

The changes in mean age show several features that are similar to those in AOU, although the trends in the upper 1,500 m are less clear. The appearance of the convectively formed GSAIW, represented by the 500–1,000 m layer (Eldevik et al., 2009; Jeansson et al., 2017) in the 1990s had a clear impact on the age, decreasing from 27 years in 1982, to 8 years in the 1990s and the 2000s, and 2 years in the 2010s. The 1,000–1,500 m layer showed a clear increase in ventilation (decrease in age) from the 1990s to the 2010s, with a mean age of 28 years in the 1990s, 16 years in the 2000s, and 6 years in the 2010s. The layer below (1,500–2,000 m) had an age of ~70 years until the 2000s, which decreased to 16 years in the 2010s. This clearly indicates that the upper 2,000 m have been

Table 1
Decadal Means (± Standard Deviations) in Potential Temperature, Salinity, Apparent Oxygen Utilization, Mean Age and C_{ant} for Main/Selected Water Masses in the Nordic Seas

Water mass	Parameters	1982	1990s	2000s	2010s
ISAIW 200–500 m	Pot. temp (°C)	−0.22 ± 0.10	−0.19 ± 0.20	−0.22 ± 0.10	−0.12 ± 0.11
	Salinity	34.890 ± 0.019	34.874 ± 0.032	34.877 ± 0.021	34.887 ± 0.016
	AOU (µmol kg⁻¹)	43.7 ± 11.0	41.7 ± 13.2	33.2 ± 10.6	29.2 ± 9.6
	Mean age (yr)	7.7 ± 6.6	25.3 ± 14.2	15.7 ± 7.1	
	C_{ant} (µmol kg⁻¹)	27.3 ± 2.6	28.6 ± 4.5	36.2 ± 3.3	
ISDW 1,500–2,000 m	Pot. temp (°C)	−0.97 ± 0.02	−0.95 ± 0.02	−0.89 ± 0.02	−0.84 ± 0.01
	Salinity	34.915 ± 0.006	34.911 ± 0.005	34.911 ± 0.002	34.912 ± 0.002
	AOU (µmol kg⁻¹)	60.5 ± 4.0	60.4 ± 5.1	59.2 ± 5.4	62.0 ± 5.0
	Mean age (yr)	70.2 ± 0.3	124.8 ± 16.1	133.6 ± 8.5	
	C_{ant} (µmol kg⁻¹)	15.9 ± 0.0	14.3 ± 1.6	15.7 ± 0.8	
GSAIW 500–1,000 m	Pot. temp (°C)	−1.12 ± 0.05	−0.87 ± 0.10	−0.76 ± 0.14	−0.40 ± 0.13
	Salinity	34.891 ± 0.003	34.879 ± 0.007	34.888 ± 0.009	34.917 ± 0.004
	AOU (µmol kg⁻¹)	43.9 ± 1.7	33.0 ± 3.9	26.2 ± 3.6	19.5 ± 2.2
	Mean age (yr)	26.9	7.8 ± 5.4	8.2 ± 3.3	1.9 ± 1.3
	C_{ant} (µmol kg⁻¹)	21.7	34.9 ± 2.2	39.3 ± 2.1	52.8 ± 1.0
GSDW 2,000–3,000 m	Pot. temp (°C)	−1.26 ± 0.02	−1.08 ± 0.05	−0.97 ± 0.08	−0.84 ± 0.07
	Salinity	34.894 ± 0.001	34.904 ± 0.003	34.909 ± 0.003	34.916 ± 0.003
	AOU (µmol kg⁻¹)	42.4 ± 1.0	54.5 ± 2.7	56.3 ± 1.8	54.5 ± 4.2
	Mean age (yr)	34.7	100.6 ± 17.2	138.4 ± 19.0	130.1 ± 50.2
	C_{ant} (µmol kg⁻¹)	20.3	16.6 ± 1.4	15.4 ± 1.9	20.9 ± 6.2
GSBW 3,000–4,000 m	Pot. temp (°C)	−1.28 ± 0.00	−1.17 ± 0.02	−1.08 ± 0.05	−0.93 ± 0.02
	Salinity	34.892 ± 0.001	34.901 ± 0.005	34.906 ± 0.003	34.916 ± 0.002
	AOU (µmol kg⁻¹)	41.9 ± 0.7	52.7 ± 2.4	55.0 ± 2.0	58.3 ± 1.1
	Mean age (yr)	37.7 ± 0.4	111.1 ± 12.4	146.1 ± 18.4	200.9 ± 6.1
	C_{ant} (µmol kg⁻¹)	19.8 ± 0.1	15.6 ± 0.7	14.7 ± 0.8	14.1 ± 0.4
NSAIW (NB) 500–1,000 m	Pot. temp (°C)	−0.15 ± 0.35	−0.36 ± 0.29	−0.37 ± 0.28	
	Salinity	34.907 ± 0.005	34.896 ± 0.007	34.893 ± 0.004	
	AOU (µmol kg⁻¹)	49.6 ± 5.3	51.8 ± 6.3	46.9 ± 3.9	
	Mean age (yr)	35.9 ± 23.2	33.5 ± 19.8	29.2 ± 12.7	
	C_{ant} (µmol kg⁻¹)	21.0 ± 3.8	27.7 ± 4.7	31.2 ± 3.8	
NSAIW (LB) 1,000–1,500 m	Pot. temp (°C)	−0.39 ± 0.24	−0.34 ± 0.31	0.10 ± 1.38	
	Salinity	34.907 ± 0.007	34.901 ± 0.006	34.918 ± 0.059	
	AOU (µmol kg⁻¹)	52.5 ± 3.6	51.8 ± 4.9	44.2 ± 11.1	
	Mean age (yr)	42.1 ± 17.3	44.1 ± 22.0	32.1 ± 18.5	
	C_{ant} (µmol kg⁻¹)	19.6 ± 2.7	24.6 ± 4.6	32.4 ± 6.7	
NSDW (NB) 3,000–4,000 m	Pot. temp (°C)	−1.05 ± 0.00	−1.03 ± 0.00	−1.02 ± 0.00	
	Salinity	34.910 ± 0.001	34.909 ± 0.003	34.911 ± 0.001	
	AOU (µmol kg⁻¹)	55.1 ± 0.8	59.5 ± 3.8	60.5 ± 0.4	
	Mean age (yr)	119.6	197.1 ± 14.3	212.1 ± 9.0	
	C_{ant} (µmol kg⁻¹)	12.1	10.5 ± 0.6	10.9 ± 0.4	
NSDW (LB) 3,000–4,000 m	Pot. temp (°C)	−1.05 ± 0.00	−1.03 ± 0.01	−0.99 ± 0.02	
	Salinity	34.909 ± 0.000	34.910 ± 0.003	34.910 ± 0.002	

Table 1
Continued

Water mass	Parameters	1982	1990s	2000s	2010s
	AOU (μmol kg^{-1})	56.6 ± 0.2	57.8 ± 2.8	60.6 ± 1.3	
	Mean age (yr)	83.5 ± 0.2	166.8 ± 10.6	196.7 ± 9.0	
	C_{ant} (μmol kg^{-1})	14.7 ± 0.0	11.7 ± 0.4	12.1 ± 0.4	

progressively more ventilated over the decades. In contrast, the mean ages of the deep waters increased considerably over the analyzed time-period, from ~40 years in 1982 to between 130 and 200 years in the 2010s. This large increase reflects the increased fraction of Arctic Ocean deep waters in the Greenland Sea following the cessation of deep-water formation in the 1980s (e.g., Karstensen et al., 2005; Schlosser et al., 1991; Somavilla et al., 2013). This will be further discussed in Section 4.2. It should be stated that the uncertainties in the mean ages as illustrated by the $\pm$ in Table 1 and the error bars in Figures 7–10 are based on the standard deviations of the means in each layer and decade. The real uncertainty, however, largely connected to the uncertainty in the applied Δ/Γ, may be much higher as indicated in Figure 4.

The concentrations of C_{ant} more than doubled at all depths above 2,000 m over the period. The change in the 1,500–2,000 m layer from the 2000s to the 2010s, was as large as 82%, due to the intense convection. The deep waters showed declining C_{ant} concentrations, except GSDW (at 2,000–3,000 m) from the 2000s to the 2010s, which increased by 36%, although with a large spread. This indicates that the ventilation, in the 2010s, reached below 2,000 m. However, the observed decreases in the mean values of both AOU and mean age are small and not significant, considering the uncertainties.

3.2.2. Iceland Sea

In the Iceland Sea (Figure 8) the trends are overall less clear than in the Greenland Sea. In the upper 1,000 m the temperature was stable over the first decades but warming occurred in the 2010s. The salinity was more variable. In the 500–1,000 m layer, which is affected by GSAIW (Jeansson et al., 2017), salinity declined from 1982 to the 2000s, and then increased in the 2010s. This recent increase is suggested to be a consequence of the positive salinity trend in the GSAIW since the 1990s. Below 1,000 m there was a warming over the entire period, but for salinity the clearest change was from the higher values in 1982 to lower values in the following decades. The salinities in the deeper part of the Iceland Sea in 1982 were higher than in any of the other basins at that time.

For AOU the only layer showing a clearly declining trend is the 200–500 m layer, which is dominated by ISAIW (Jeansson et al., 2017). In the layer below, AOU has decreased slightly, but the change is smaller than the uncertainties. The deep waters showed minor changes over the analyzed period.

The mean age varied over the decades. Above 1,500 m, waters were older in the 1990s than in both the 1980s and the 2000s. The Iceland Sea Deep Water (below 1,500 m) increased considerably in mean age from 1982 (70 years) to the 1990s and the 2000s (125–134 years). As in the Greenland Sea, this can only be explained by a larger fraction of older deep water from the Arctic Ocean. Unfortunately, there are no tracer data from the 2010s available for the Iceland Sea.

The change in C_{ant} was minor from 1982 to the 1990s, but the 2000s displayed a rather considerable increase compared to the 1990s, at all depths above 1,500 m, of 24%–29%.

3.2.3. Norwegian Basin

In the Norwegian Basin (Figure 9) the 200–500 m layer is affected by warm (~2°C) Atlantic Water. The mean salinity varied over the decades, with the 1990s being fresher. The layer below is dominated by NSAIW (e.g., Jeansson et al., 2017), and got fresher with time. Some freshening could also be observed in the layer below. All waters below 1,500 m showed a slight warming over the decades (Table S4 in Supporting Information S1).

For AOU there is a clear difference between the relatively well ventilated upper 500 m and waters below, which had much higher AOU. No trends are evident in the upper 1,500 m, but the deep waters all had lower values in 1982 than in the more recent decades. The same evolution is seen in mean age. The clearest change was the significant increase from 1982 to the 1990s/2000s, indicating an increased fraction of older deep water from the Arctic Ocean, in the later decades. The age of the NSDW in the 2000s, below 2,000 m, was ~220–240 years. These are the oldest waters of the study area (Table 1).

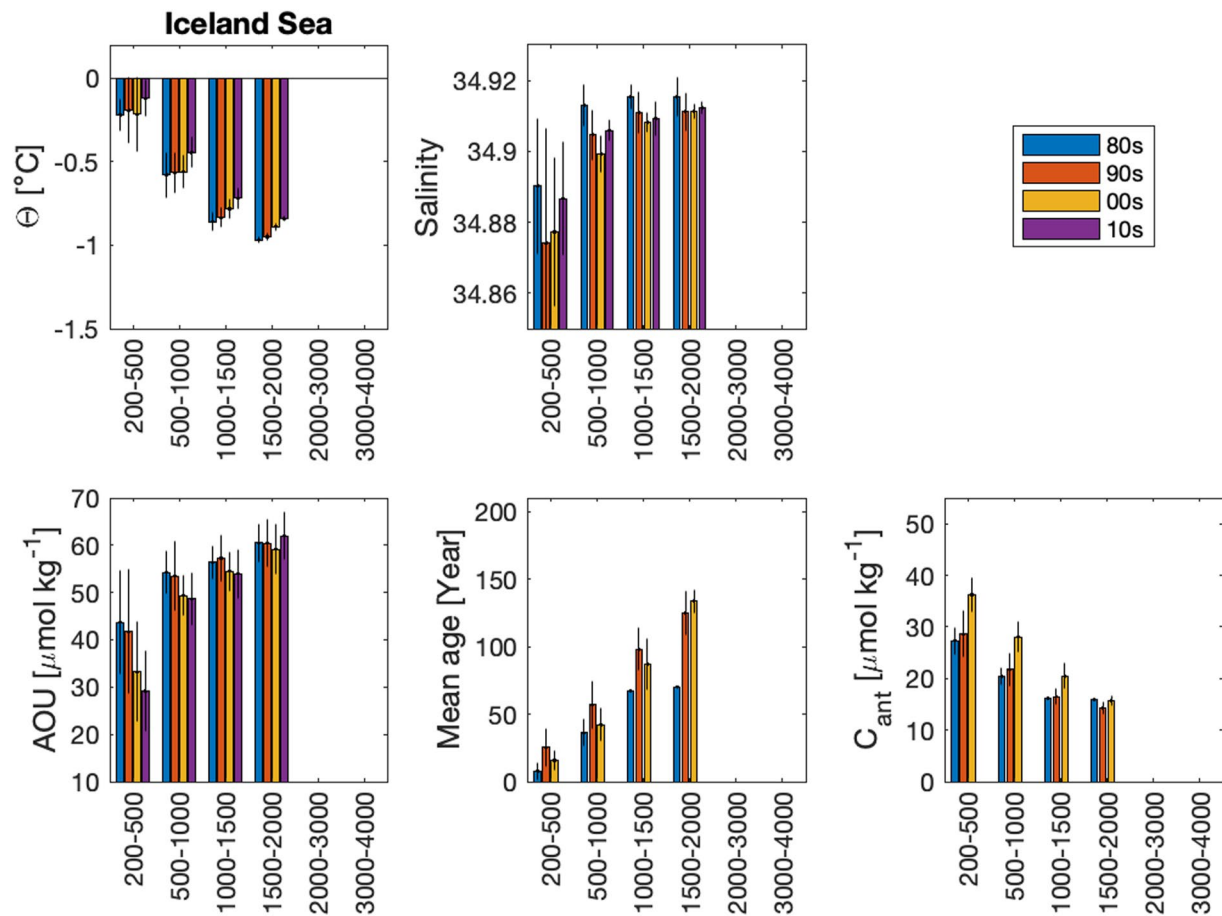**Figure 8.** Decadal changes (comparing 1982, the 1990s, the 2000s, and the 2010s) in potential temperature, salinity, AOU, mean age and C_{ant} for different depth layers in the Iceland Sea. The color coding is the same as in Figure 11. The error bars indicate the standard deviations of the decadal means for each layer.

The change in C_{ant} was clear in the upper 1,500 m, with the greatest increase in the NSAIW layer of ~50% from 1982 to the 2000s. There were only minor changes in the deeper waters.

It should be pointed out that the data coverage in this basin is the lowest of all the four evaluated basins, with 2002 being the last sampled year in the GLODAPv2.2019 data product (see Section 2).

3.2.4. Lofoten Basin

The Lofoten Basin holds a thick layer of Atlantic Water, clearly seen in the upper 1,000 m (Figure 10). The upper 500 m was clearly warmer in the 1990s/2000s than in 1982, while the mean temperature of the layer below increased every decade. However, the variability in each decade was large in this layer, seen from the magnitude of the standard deviations. Thus, there is no significant trend. The salinity in the 200–500 m layer was markedly higher in the 2000s compared to the earlier decades. The mean salinity of the 500–1,000 m layer was clearly higher in the 2000s, but again, with no significant trend considering the uncertainty in the estimates. The 1,000–1,500 m layer is dominated by NSAIW (Jeansson et al., 2017), and was colder and fresher than the upper 1,000 m. The salinity was decreasing slightly from 1982 to the 1990s, but the water became warmer, and saltier in the 2000s. It is unclear whether this reflects a deeper Atlantic Water layer or property changes of the NSAIW. Note that the standard deviations in especially the 2000s are much larger for temperature and salinity in this layer compared to the other decades, making the change statistically non-significant. The 1,500–2,000 m layer showed a small freshening trend, but also became warmer with time. This warming was also seen in the deep waters.

In AOU there was a strong gradient from the upper layers to 1,500 m. The only obvious change in the mean values with time was the decrease in the 1,000–1,500 m layer from the 1990s to the 2000s, although within the uncertainty. The deep waters only showed minor changes, with a possible, but not statistically significant, increase in AOU with time.
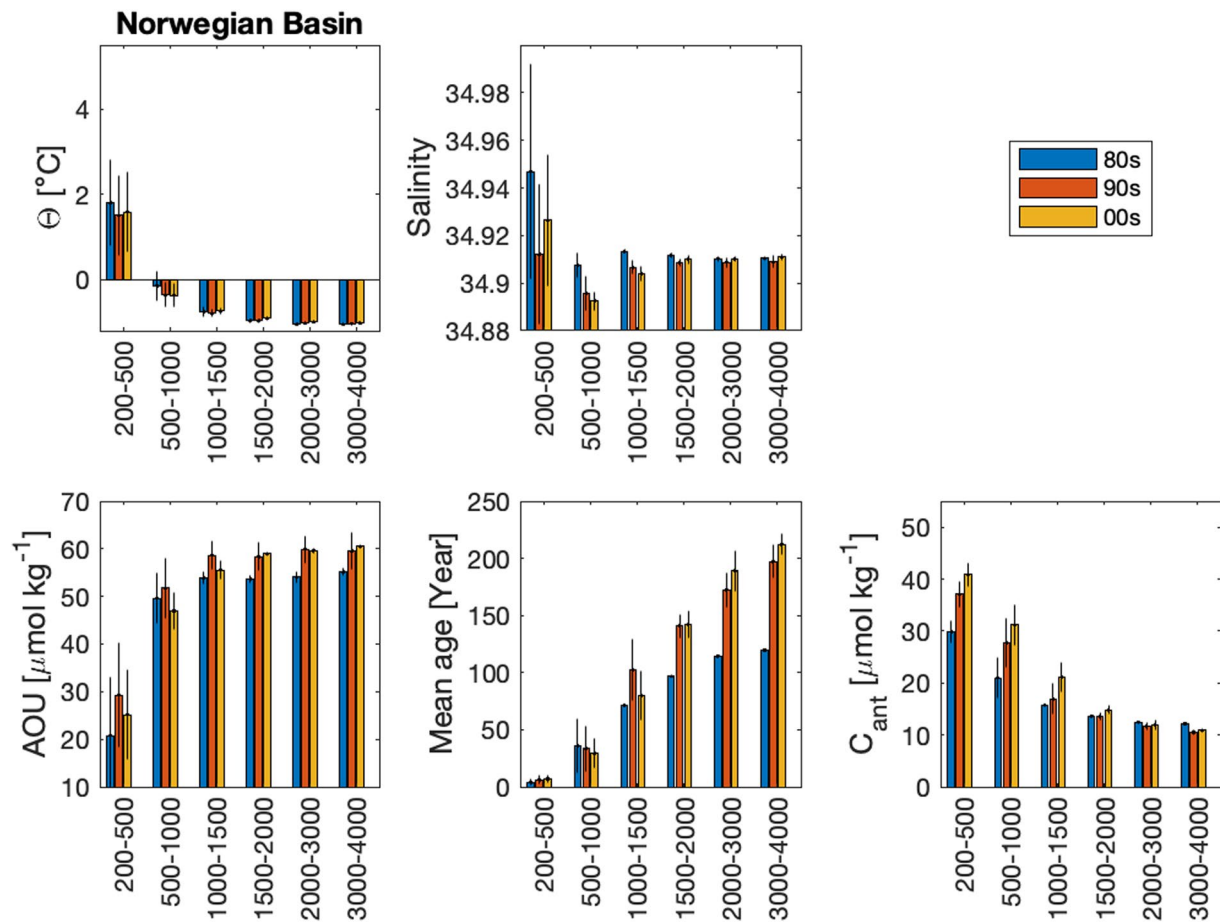
Figure 9. Decadal changes (comparing 1982, the 1990s, the 2000s, and the 2010s) in potential temperature, salinity, AOU, mean age and C_{ant} for different depth layers in the Norwegian Basin. The color coding is the same as in Figure 11. The error bars indicate the standard deviations of the decadal means for each layer.

The mean age in the upper 1,000 m was stable and low. The NSAIW layer at 1,000–1,500 m showed a small decrease from the 1990s to the 2000s, but within the uncertainty. The evolution of the deep waters (>1,500 m) in the Lofoten Basin was similar to that in the other basins, with a stronger depth gradient with time, from close to homogeneous ages in 1982 (∼80 years) to clearly older water at depth, reaching ∼200 years in the 2000s. For C_{ant}, all depths above 2,000 m showed increased concentrations with time. The largest change is seen in the NSAIW layer (1,000–1,500 m), with 65% increase in C_{ant} from 1982 to 2000s, but even the layer below had an increase of 35% over the same period. The deep-water concentrations were lower in the later decades, in agreement with the larger presence of older water.

3.3. Decadal Variability in the Column Inventory of C_{ant}

To evaluate the impact of the described concentration changes on the inventory of C_{ant} in the Nordic Seas basins, we compare the mean decadal specific column inventories of C_{ant} for each basin (see Section 2 for details). The inventories are summarized in Table 2 and Figure 11. In the 1990s, the increase (from the 1980s) in the Arctic domain (i.e., the Greenland and Iceland Seas) was rather modest (8%–10%). The increase in the Norwegian Sea was somewhat larger; 12% in the Norwegian Basin and 14% in the Lofoten Basin.

In comparison, the atmospheric C_{ant} increase was 31% over this period (between 1982 and 1995). It is only at constant ventilation that the water column concentrations, and thus the inventory, would be expected to increase at the same relative rate as the atmospheric. However, the column inventories relate to each other as an indicator of the overall ventilation state of the basins. In the 2000s, the changes were overall much larger. The increase in the Arctic domain was 14%–17%, and the Lofoten Basin inventory increased by 20% over the same period, which is similar to the atmospheric increase from 1995 to 2005 (22%). The change in the Norwegian Basin, however,
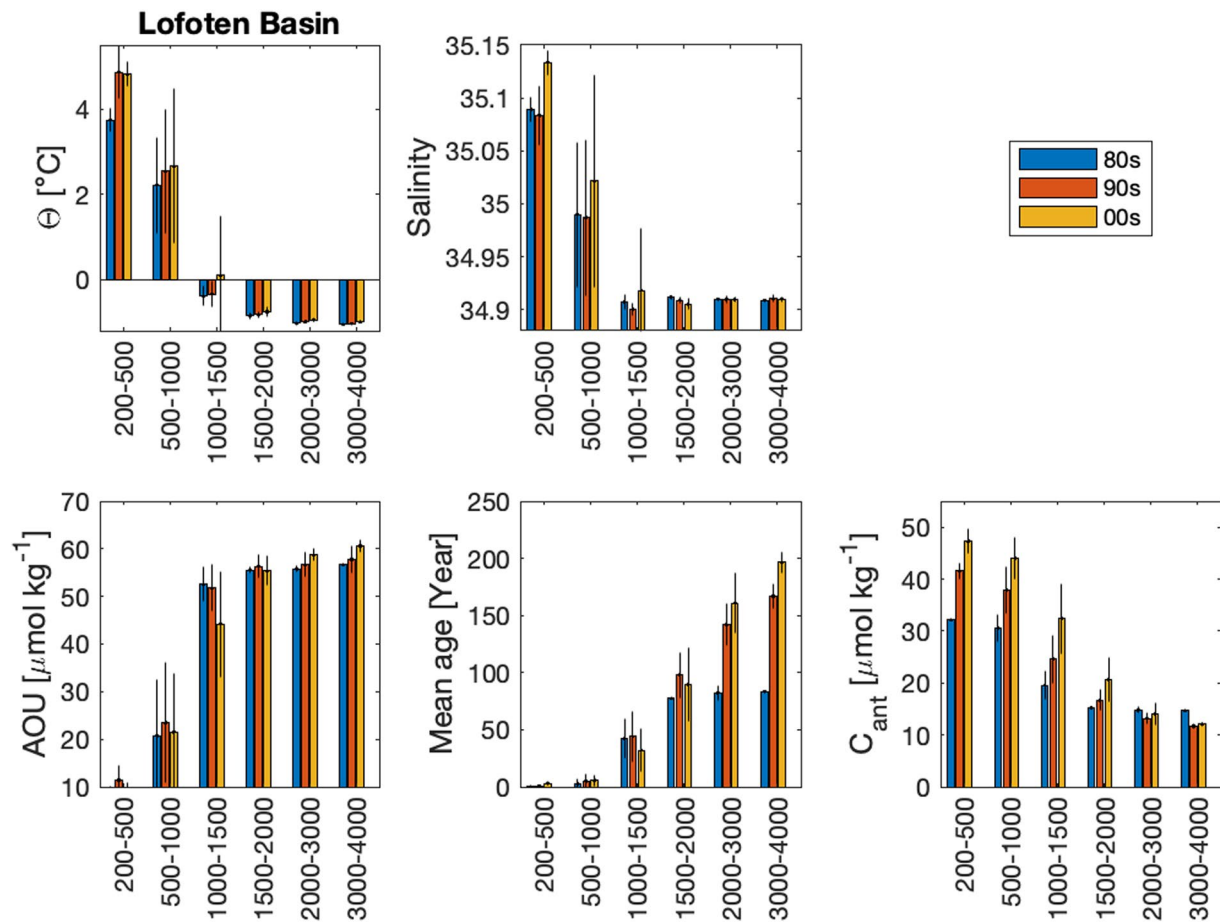
Figure 10. Decadal changes (comparing 1982, the 1990s, the 2000s, and the 2010s) in potential temperature, salinity, AOU, mean age and C_{ant} for different depth layers in the Lofoten Basin. The color coding is the same as in Figure 11. The error bars indicate the standard deviations of the decadal means for each layer.

Table 2
Column Inventory (mol m^{-2}) of C_{ant} in the Different Basins of the Nordic Seas, for Different Decades

	1982	1990s	2000s	2010s (2016)
$\Delta\ C_{ant,atm}$ (%)[a]	–	31	22	24
Greenland Sea	82.2	88.7 ± 3.0	100.9 ± 7.9	135.2
Rel. change (%)	–	7.9	13.7	34.0
Iceland Sea	40.2	44.1 ± 3.3	51.7 ± 1.7	–
Rel. change (%)	–	9.7	17.2	–
Norwegian Basin	61.5	68.9 ± 3.3	74.8 ± 2.4	–
Rel. change (%)	–	12.0	8.6	–
Lofoten Basin	69.9	80.0 ± 4.4	96.0 ± 5.6	–
Rel. change (%)	–	14.4	20.0	–

Note. The presented standard deviations for the 1990s, 2000s, and 2010s (2016) are the variability among the annual inventories over each decade. The relative change (in percent) is the change from the previous decade.
[a]This marks the relative atmospheric change in C_{ant} from 1982 to 1995, 1995 to 2005, and 2005 to 2016, respectively.

was ~9%, but then again, for this basin we only have data until 2002. The inventory in the Lofoten Basin in the 2000s is not statistically different from the Greenland Sea inventory for the same decade. The Greenland Sea inventory in 2016 is 34% larger than the mean in the 2000s, which indicates a faster growth rate than the atmospheric increase from 2005 to 2016 (24%). This is another clear illustration of the stronger ventilation of the Greenland Sea in the 2010s.

3.4. Linking Ventilation and C_{ant} Changes

To get a better understanding of the connection between ventilation and the amount of C_{ant} in the Nordic Seas, we explore the relationships among decadal changes in AOU, mean age, and C_{ant} in the different basins. We illustrate this in Figure 12, where the left column compares changes in mean age and in AOU, and the right column compares changes in C_{ant} and in AOU, for each basin. Each panel is divided into four quarters where, for the left column, the lower left quarter (a) shows negative changes in both AOU and in mean age (i.e., the clearest sign of ventilation), the upper left quarter (b) shows negative changes in AOU but positive changes in mean age, the upper right quarter (c) shows positive change in both mean age and AOU (i.e., clearest signal of waters getting older, and the lower right quarter (d) shows positive changes in AOU and negative changes in mean age. For the right column it is
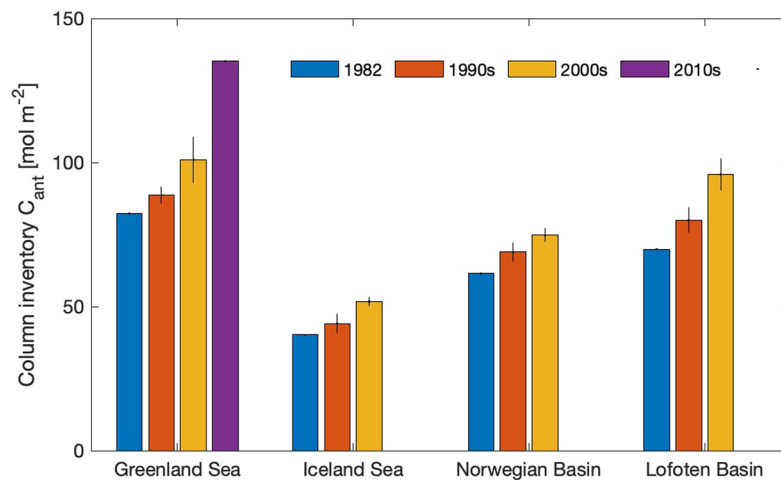
Figure 11. Decadal mean evolution in column inventory of C_{ant} in the four main basins in the Nordic Seas. The error bars indicate the standard deviations of the decadal means.

the upper left quarter that shows the clearest signal of ventilation-driven increase in C_{ant} (positive change in C_{ant} and negative change in AOU).

For the Greenland Sea there is a clear development over time that more layers are moving from the quarter iii (i.e., an aging of the water masses; left column) toward the quarter i, illustrating the increased ventilation. In the 2010s only the deepest layer remains in the non-ventilated quarter. The largest change is seen for the 1,500–2,000 m layer from the 2000s to the 2010s, which is the case for AOU, mean age, and C_{ant}; the age decrease ~50 years and the concentration of C_{ant} increase with almost 15 µmol kg^{-1}.

The changes in the Iceland Sea between 1982 and the 1990s are all close to "0" regarding AOU, but with an aging of the deeper layers; the age of the deepest layer (>1,500 m) increase by ~50 years. The changes in C_{ant} are all very small, and centered between the quarters. In the 2000s most layers, except the deepest one, move into the "ventilation quarter," with lower AOU and mean age and higher C_{ant}. This is clearest in the 200–500 m layer (dominated by ISAIW), but also for the layer below (affected by GSAIW).

The Norwegian Basin displays a lack of ventilation between 1982 and the 1990s, with all AOU and mean age changes in/around the quarter iii, and with some very large increases in age of the deeper layers. Still, there are some increases in C_{ant} in the layers between 200 and 1,000 m. In the 2000s all layers have moved toward the center or into the quarter i, which is clearest for mean age of the 1,000–1,500 m layer.

The development in the Lofoten Basin is somewhat similar to the Norwegian Basin. However, while this is especially true for the depths below 2,000 m, a larger part of the water column in the 1990s is closer to the "0" axis for AOU change, and the upper 1,500 m also displays no change in mean age, and a positive change in C_{ant}. Also in this basin, more layers in the 2000s are found in or close to the quarter i, with the clearest change for the 1,000–1,500 m layer for both mean age and C_{ant}.

4. Discussion

4.1. Intermediate Layers

The intermediate layers are where ventilation changes would first be detected since the upper layers are expected to be well ventilated. The most obvious candidate is of course the Greenland Sea, where numerous studies have documented the development in convection (e.g., Brakstad et al., 2019; Karstensen et al., 2005; Lauvset et al., 2018; Ronski & Budéus, 2005). This basin shows a very strong transformation from the 1980s to the 2010s. While intermediate depths (500–1,000 m) were part of the rather homogenous deeper water column in 1982 the cessation of deep-reaching convection (e.g., Karstensen et al., 2005; Schlosser et al., 1991; Somavilla et al., 2013) led to a more intermediate-reaching ventilation, and the emergence of the cold and fresh GSAIW in the 1990s. The hydrographic properties of this water mass have changed considerably in the recent decades,
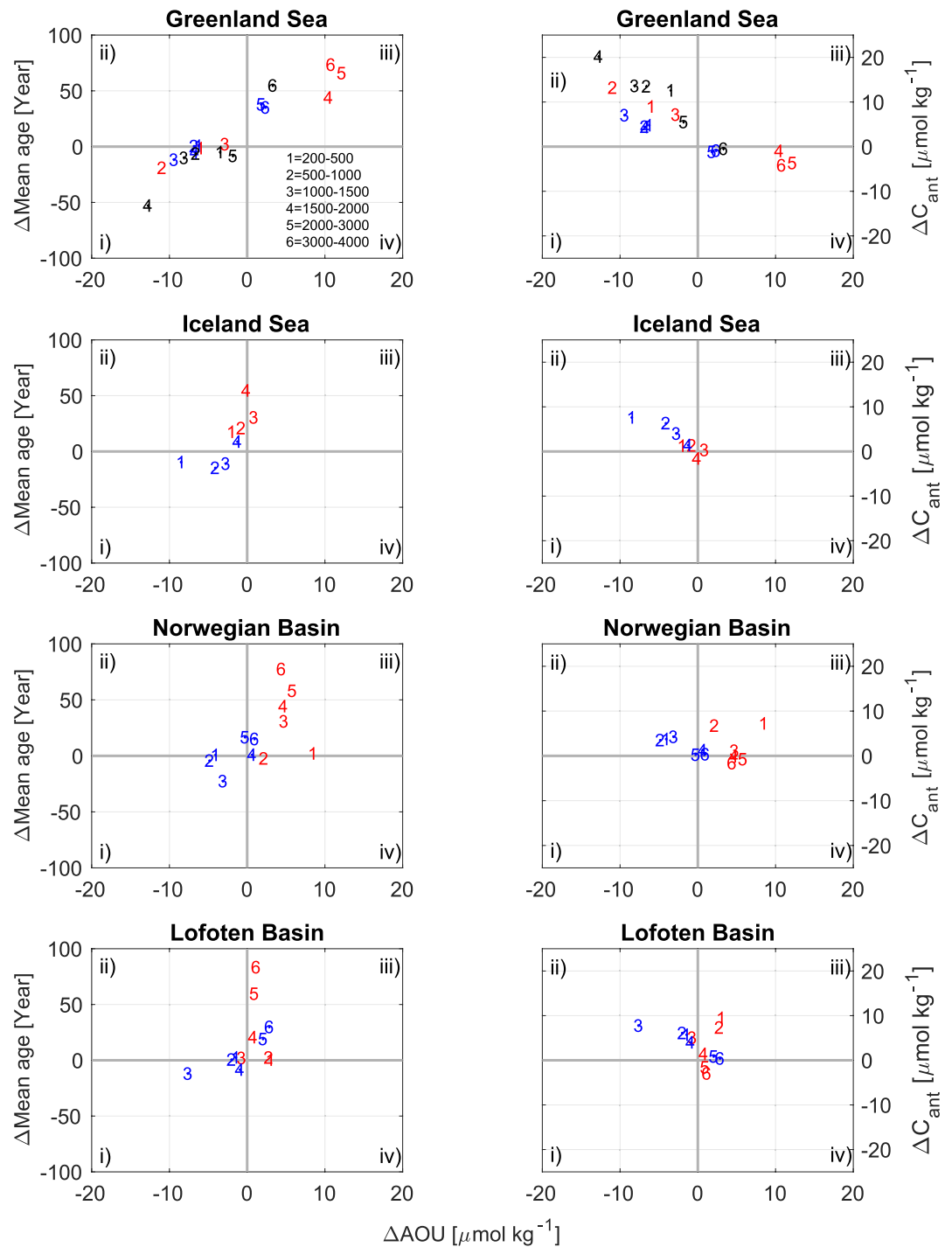
Figure 12. Decadal changes in AOU versus mean age (left column), and AOU versus C_{ant} (right column), in the four main Nordic Seas basins (one row per basins). The change in each analyzed depth layer is displayed as a number (1–6), representing the evaluated depth layers (defined in the upper left panel), color coded by decade: red shows the change between 1982 and the 1990s, blue the change between the 1990s and the 2000s, and black the change between the 2000s and the 2010s. The roman numbering (a–d) refer to the divided quarters. See text for further clarification.

becoming warmer and saltier (Table 1), as has also been documented by, for example, Brakstad et al. (2019) and Lauvset et al. (2018). The vertical extent of the GSAIW is also increasing (e.g., Jeansson et al., 2017). There are indications in the 2010s that the convection has started to affect the upper part of the deep water, below 2,000 m. This would be a clear shift from the situation during the last decades, but more recent observations are needed

to clarify if this is indeed an ongoing trend. Compared to the Greenland Sea, the other basins of the Nordic Seas host a rather thin layer of intermediate water. This makes it more challenging to find clear evidence of significant ventilation changes, especially since the interannual variability can be high. Our focus on decadal means also leads to rather large spread in the results over each decade, and thus overlapping ranges. Still, there are many indications that while the 1990s was a period of modest to slow ventilation, this changed in the 2000s. We hypothesize that this is due to the spreading of GSAIW to the different basins (e.g., Blindheim, 1990; Jeansson et al., 2017), but the changes in AOU and mean age of the NSAIW in either of the Norwegian Basins are not statistically significant. The recent property changes of GSAIW should be possible to follow as these propagated around the Nordic Seas with the spreading of GSAIW. However, this is difficult to assess from the present study since we here focus on the central basins.

4.2. Deep Waters

The most obvious change in the deep waters was the steadily increasing ages with time. While the mean age range found in 1982 was between ∼40 and 120 years, the range in the 2000s was between ∼130 and ∼210 years. Furthermore, the bottom waters in the Greenland Sea became ∼50 years older between the 2000s and the 2010s. This is far greater than a cessation of deep-water formation would give, approximately 10 years older waters per decade. The only plausible explanation is an increased fraction of older water, which must come from the Arctic Ocean (or an error in the assumption of the shape of the TTD, i.e., the Δ/Γ ratio, or/and that the ratio is time-invariant). These waters enter the Nordic Seas via the Fram Strait, where the ages of the Arctic Ocean deep waters are in the range 170–250 years (Stöven et al., 2016). The evolution of the GSBW in the 2010s is different from that of the GSDW; the former continued the trend of aging, while the latter showed some signs of ventilation, as discussed above. The gradual transformation from younger "classic" locally formed GSBW into older more Arctic Ocean-type deep water is seen in many properties (Figure 13). The initial GSBW in the early 1980s was cold and relatively fresh, low in silicate and relatively high in oxygen. These properties changed almost linearly over the evaluated period, toward higher temperature, salinity, silicate, and lower oxygen. These trends also followed a trend of increased age. The increased fraction of Arctic Ocean deep water in the Greenland Sea can be evaluated with a simple two end-member mixing scenario, where one is the Eurasian Basin Deep Water (EBDW; Arctic Ocean), and the second the "classic" GSBW from 1982 (Table 1: $\Theta = -1.28°C$; $S = 34.892$; $AOU = 41.9$ µmol kg^{-1}; mean age (from CFC-12) = 38 years). Using the properties of EBDW from Jeansson et al. (2008) ($\Theta = -0.87°C$; $S = 34.923$; $AOU = 56.3$ µmol kg^{-1}; mean age (from CFC-12) = 349 years), assuming that these are representative for the whole period, we can calculate the fraction of the classic GSBW and EBDW needed to explain the GSBW properties in 1990, the 2000s, and the 2010s (Table 1). Using only Θ and S (separately), the resulting fractions (in %) of EBDW is ∼30%, 45%–50%, and 77%–85%, in the 1990s, the 2000s, and the 2010s, respectively. If we conduct the same calculation using mean age, adjusted for the time passed since 1982 (i.e., deduct this time from the mean ages of the different decades), the fraction of EBDW is 32%, 45%, and 70%, in the 1990s, the 2000s, and the 2010s, respectively. This is in very good agreement with the results from the hydrography. This agreement supports the mixing evolution with an increased fraction of Arctic Ocean deep water in the deep Greenland Sea and rules out any considerable error in the Δ/Γ ratio as an explanation for the large increase in mean age with time. If we use AOU instead, the results are very different, with an EBDW fraction of 75% already in the 1990s, and ∼90% in the 2000s. This is likely due to the much smaller gradients in AOU among the deep waters in the region (∼53–58 µmol kg^{-1} for GSBW after the 1990s, and ∼56 µmol kg^{-1} for EBDW in 2002), despite a large range in mean age. Thus, even though the uncertainty in mean age is larger at higher ages (see Figure 7) it seems to be a better tracer to identify water mass changes in the deep water in the studied region, compared to AOU. The small deep-water gradient in AOU may partly be explained by the low primary production and consequentially remineralization in the Arctic Ocean, but also in the Nordic Seas due to the relatively young ages compared to deep waters in the global ocean.

An increased fraction of Arctic Ocean deep water is also the only plausible explanation for the older ages found in the deep parts outside the Greenland Sea, especially when comparing 1982 with the 1990s and 2000s. The Arctic Ocean deep water can reach these basins either via the boundary currents (e.g., Blindheim & Rey, 2004), via the Greenland Sea through openings in the Jan Mayen Fracture Zone (to the Iceland Sea) or through the Jan Mayen Channel (to the Norwegian Sea; e.g., Østerhus & Gammelsrød, 1999; Q. Shao et al., 2019). We do not attempt to identify the specific pathways with this basin-centered analysis, but some combination of the pathways may be plausible.
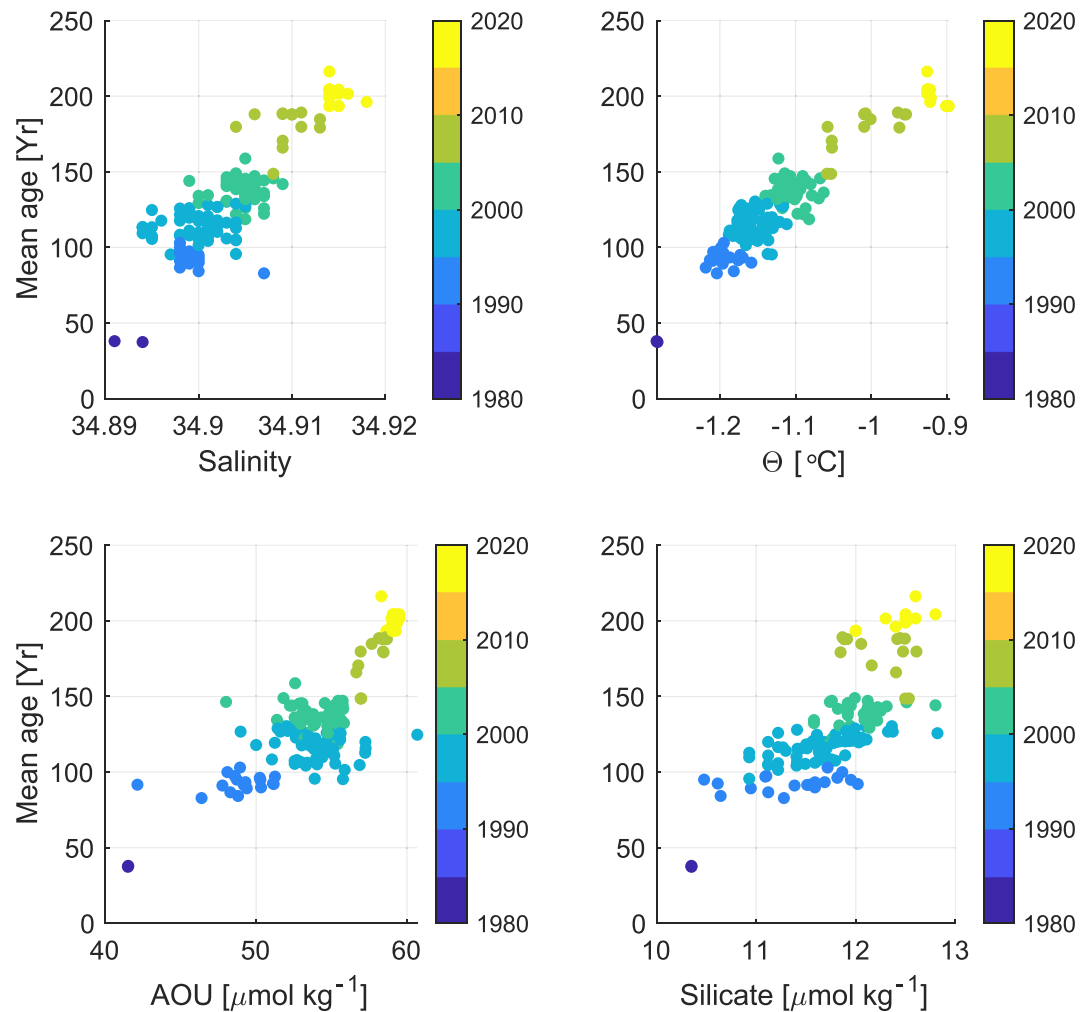
Figure 13. Evolution of the Greenland Sea Bottom Water (below 3,000 m) in the Greenland Sea, from 1982 to 2016. The evolution of salinity (upper left), potential temperature (upper right), AOU (lower left), and silicate (lower right), are plotted against mean age. The color coding indicates time of observation.

4.3. The Impact of Ventilation State on the Accumulation of C_{ant}

Ventilation brings surface properties to deeper layers, which is important for the sequestration of C_{ant} in the ocean. At steady-state ventilation the rate in accumulation of C_{ant} will be proportional to the atmospheric increase. At a stronger (reduced) ventilation the accumulation will be faster (slower). In the Greenland Sea the trend of stronger and deeper convection with time results in an increased inventory of C_{ant}. A clear example is the 1,500–2,000 m layer, which in the earlier decades was part of the deep water due to the shallower convection, but ventilated in the later decades as the convection reached deeper. Consequently, this is where the ventilation signal is the strongest (between the 2000s and the 2010s) and also the increase in the concentration of C_{ant} (Figure 12). This also led to a larger increase in the inventory compared to the previous decades (Figure 11). This is also a result of the increase in C_{ant} below 2,000 m. The Lofoten Basin had also a relatively fast accumulation in the 2000s compared to earlier decades. Since this basin has a thick layer of Atlantic Water in the upper ~1,000 m, which is expected to be in phase with the atmosphere, this rate change is most likely linked to advection of GSAIW. Indeed, the largest increase in both ventilation and C_{ant} is seen in the 1,000–1,500 m layer (Figure 12), which is dominated by GSAIW. The change in the Iceland Sea and Norwegian Basin is closer to steady state. Nevertheless, as indicated in Figure 12, all basins show a general increase in ventilation state in the 2000s (and later, when relevant) compared to the 1990s, and this is followed by an increased rate in C_{ant} accumulation. It will be very interesting to see if this development will continue.

5. Conclusions

This study has presented an evaluation of decadal changes in ventilation in the Nordic Seas, based on both TTD-derived mean ages and apparent oxygen utilization (AOU), and changes in concentrations and column inventories of anthropogenic carbon (C_{ant}). In terms of ventilation, the Nordic Seas have gone through some clear shifts from 1982 to the 2010s. This is particularly evident in the Greenland Sea, which changed from a rather well-ventilated basin at all depths in the early 1980s, to a much shallower ventilation in the 1990s, and a re-vitalization of the convection in the 2000s in the upper 1,500 m. This continued in the 2010s, accompanied with considerable change in the hydrographic properties of the intermediate waters during the recent decade. The ventilation of the other main basins of the Nordic Seas was more variable over the studied period, with the 1990s generally less, and the 2000s more, ventilated. We hypothesize that the stronger ventilation typically found in the Nordic Seas in the 2000s is linked to the advection of intermediate water from the Greenland Sea. However, this needs to be evaluated further, and is perhaps best done within a modeling framework. The deep waters of the Nordic Seas, however, show a trend of increased age with time. The magnitude (typically more than 50 years per decade) is much larger than a cessation of deep convection would give. This must therefore be the result of an increased fraction of older deep water from the Arctic Ocean, slowly filling the deep Nordic Seas basins and reducing the gradients between them.

The changes in C_{ant} are clearly connected to the level of ventilation; the stronger the ventilation, the larger the increase in C_{ant} concentration. This is also reflected in the inventory of C_{ant}. The inventory increases from 1982 to 1990s in the four basins were rather modest (8%–14%), while the increases from the 1990s to the 2000s were in the range 14%–20% (except the Norwegian Basin with less data). The Greenland Sea is the only basin with tracer data also in the 2010s, and here the change in both ventilation and C_{ant} into that decade was stronger than in any other part of the Nordic Seas over the analyzed period, and the relative change in C_{ant} inventory (34%) even surpassed the atmospheric increase (24%).

The contribution of dense overflows from the Nordic Seas is a major component of the Atlantic Meridional Overturning Circulation (AMOC) (e.g., Chafik & Rossby, 2019). AMOC is a critical process controlling the Earth's climate. Thus, it is very important to sustain a well-covered observational network in this region.

Data Availability Statement

The used data from the GLODAPv2.2019 data product (Olsen et al., 2019) can be found at https://www.ncei.noaa.gov/access/ocean-carbon-acidification-data-system/oceans/GLODAPv2_2019/. The Iceland Sea CFC time-series data (Ólafsson et al., 2023) are available at https://ncei.noaa.gov/archive/accession/0276771. These data will be included in the next version of GLODAP (GLODAPv2.2023).

References

Anderson, L. G., Chierici, M., Fogelqvist, E., & Johannessen, T. (2000). Flux of anthropogenic carbon into the deep Greenland Sea. *Journal of Geophysical Research*, *105*(C6), 14339–14345. https://doi.org/10.1029/1999JC900276

Atamanchuck, D., Koelling, J., Send, U., & Wallace, D. W. R. (2020). Rapid transfer of oxygen to the deep ocean mediated by bubbles. *Nature Geoscience*, *13*(3), 232–237. https://doi.org/10.1038/s41561-020-0532-2

Blindheim, J. (1990). Arctic intermediate water in the Norwegian Sea. *Deep-Sea Research*, *37*(9), 1475–1489. https://doi.org/10.1016/0198-0149(90)90138-L

Blindheim, J., & Rey, F. (2004). Water-mass formation and distribution in the Nordic Seas during the 1990s. *ICES Journal of Marine Science*, *61*(5), 846–863. https://doi.org/10.1016/j.icesjms.2004.05.003

Bourke, R. H., Paquette, R. G., & Blythe, R. F. (1992). The Jan Mayen Current of the Greenland Sea. *Journal of Geophysical Research*, *97*(C5), 7241–7250. https://doi.org/10.1029/92JC00150

Brakstad, A., Våge, K., Håvik, L., & Moore, G. W. K. (2019). Water mass transformation in the Greenland Sea during the period 1986–2016. *Journal of Physical Oceanography*, *49*(1), 121–140. https://doi.org/10.1175/jpo-d-17-0273.1

Bullister, J. L. (2015). Atmospheric histories (1765-2015) for CFC-11, CFC-12, CFC-113 Technical Report NDP-095. *Carbon Dioxide Information Analysis Center, Oak Ridge National Laboratory, US Department of Energy*. https://doi.org/10.3334/CDIAC/otg.CFC_ATM_Hist_2015

Bullister, J. L., & Weiss, R. F. (1983). Anthropogenic chlorofluoromethanes in the Greenland and Norwegian Seas. *Science*, *221*(4607), 265–268. https://doi.org/10.1126/science.221.4607.265

Bullister, J. L., Wisegarver, D. P., & Menzia, F. A. (2002). The solubility of sulfur hexafluoride in water and seawater. *Deep-Sea Research Part I*, *49*(1), 175–187. https://doi.org/10.1016/S0967-0637(01)00051-6

Chafik, L., & Rossby, T. (2019). Volume, heat, and freshwater divergences in the subpolar North Atlantic suggest the Nordic Seas as key to the state of the meridional overturning circulation. *Geophysical Research Letters*, *46*(9), 4799–4808. https://doi.org/10.1029/2019gl082110

Dickson, A. G., & Millero, F. J. (1987). A comparison of the equilibrium constants for the dissociation of carbonic acid in seawater media. *Deep-Sea Research, Part A: Oceanographic Research Papers*, *34*(10), 1733–1743. https://doi.org/10.1016/0198-0149(87)90021-5

Dickson, R. R., & Brown, J. (1994). The production of North Atlantic Deep Water: Sources, rates, and pathways. *Journal of Geophysical Research*, *99*(C6), 12319–12341. https://doi.org/10.1029/94JC00530

Doney, S. C., & Bullister, J. L. (1992). A chlorofluorocarbon section in the eastern North Atlantic. *Deep-Sea Research, Part A: Oceanographic Research Papers*, *39*(11–12A), 1857–1883. https://doi.org/10.1016/0198-0149(92)90003-C

Ebser, S., Kersting, A., Stöven, T., Feng, Z., Ringena, L., Schmidt, M., et al. (2018). ³⁹Ar dating with small samples provides new key constraints on ocean ventilation. *Nature Communications*, *9*(1), 5046. https://doi.org/10.1038/s41467-018-07465-7

Eldevik, T., Nilsen, J. E. O., Iovino, D., Olsson, K. A., Sando, A. B., & Drange, H. (2009). Observed sources and variability of Nordic seas overflow. *Nature Geoscience*, *2*(6), 406–410. https://doi.org/10.1038/ngeo1518

Fine, R. A., Peacock, S., Maltrud, M. E., & Bryan, F. O. (2017). A new look at ocean ventilation time scales and their uncertainties. *Journal of Geophysical Research: Oceans*, *122*(5), 3771–3798. https://doi.org/10.1002/2016JC012529

Friis, K., Körtzinger, A., Pätsch, J., & Wallace, D. W. R. (2005). On the temporal increase of anthropogenic CO₂ in the subpolar North Atlantic. *Deep Sea Research Part I: Oceanographic Research Papers*, *52*(5), 681–698. https://doi.org/10.1016/j.dsr.2004.11.017

Fritsch, F. N., & Carlson, R. E. (1980). Monotone piecewise cubic interpolation. *SIAM Journal on Numerical Analysis*, *17*(2), 238–246. https://doi.org/10.1137/0717021

Fröb, F., Olsen, A., Våge, K., Moore, G. W. K., Yashayaev, I., Jeansson, E., & Rajasakaren, B. (2016). Irminger Sea deep convection injects oxygen and anthropogenic carbon to the ocean interior. *Nature Communications*, *7*(1), 13244. https://doi.org/10.1038/ncomms13244

Gammon, R., Cline, J., & Wisegarver, D. (1982). Chlorofluoromethanes in the Northeast Pacific Ocean: Measured vertical distributions and application as transient tracers of upper ocean mixing. *Journal of Geophysical Research*, *87*(C12), 9441–9454. https://doi.org/10.1029/JC087iC12p09441

Gruber, N., Clement, D., Carter, B. R., Feely, R. A., van Heuven, S., Hoppema, M., et al. (2019). The oceanic sink for anthropogenic CO₂ from 1994 to 2007. *Science*, *363*(6432), 1193–1199. https://doi.org/10.1126/science.aau5153

Haine, T. W. N., & Hall, T. M. (2002). A generalized transport theory: Water-mass composition and age. *Journal of Physical Oceanography*, *32*(6), 1932–1946. https://doi.org/10.1175/1520-0485(2002)032<1932:Agttwm>2.0.Co;2

Hall, T. M., Haine, T. W. N., & Waugh, D. W. (2002). Inferring the concentration of anthropogenic carbon in the ocean from tracers. *Global Biogeochemical Cycles*, *16*(4), 1131. https://doi.org/10.1029/2001GB001835

He, Y.-C., Tjiputra, J., Langehaug, H. R., Jeansson, E., Gao, Y., Schwinger, J., & Olsen, A. (2018). A model-based evaluation of the inverse Gaussian transit-time distribution method for inferring anthropogenic carbon storage in the ocean. *Journal of Geophysical Research: Oceans*, *123*(3), 1777–1800. https://doi.org/10.1002/2017JC013504

Holliday, N. P., Hughes, S. L., Bacon, S., Beszczynska-Möller, A., Hansen, B., Lavin, A., et al. (2008). Reversal of the 1960s to 1990s freshening trend in the northeast North Atlantic and Nordic Seas. *Geophysical Research Letters*, *35*(3), L03614. https://doi.org/10.1029/2007GL032675

Ito, T., Follows, M. J., & Boyle, E. A. (2004). Is AOU a good measure of respiration in the oceans? *Geophysical Research Letters*, *31*(17), L17305. https://doi.org/10.1029/2004gl020900

Jeansson, E., Bellerby, R. G. J., Skjelvan, I., Frigstad, H., Ólafsdóttir, S. R., & Ólafsson, J. (2015). Fluxes of carbon and nutrients to the Iceland Sea surface layer and inferred primary productivity and stoichiometry. *Biogeosciences*, *12*(3), 875–885. https://doi.org/10.5194/bg-12-875-2015

Jeansson, E., Jutterström, S., Rudels, B., Anderson, L. G., Olsson, K. A., Jones, E. P., et al. (2008). Sources to the East Greenland Current and its contribution to the Denmark Strait overflow. *Progress in Oceanography*, *78*(1), 12–28. https://doi.org/10.1016/j.pocean.2007.08.031

Jeansson, E., Olsen, A., & Jutterström, S. (2017). Arctic intermediate water in the Nordic Seas, 1991–2009. *Deep Sea Research Part I: Oceanographic Research Papers*, *128*(Supplement C), 82–97. https://doi.org/10.1016/j.dsr.2017.08.013

Jeansson, E., Olsson, K. A., Messias, M.-J., Kasajima, Y., & Johannessen, T. (2009). Evidence of Greenland Sea water in the Iceland Basin. *Geophysical Research Letters*, *36*(9), L09605. https://doi.org/10.1029/2009GL037988

Jeansson, E., Olsson, K. A., Tanhua, T., & Bullister, J. L. (2010). Nordic Seas and Arctic Ocean CFC data in CARINA. *Earth System Science Data*, *2*(1), 79–97. https://doi.org/10.5194/essd-2-79-2010

Jutterström, S., Jeansson, E., Anderson, L. G., Bellerby, R., Jones, E. P., Smethie, W. M., & Swift, J. H. (2008). Evaluation of anthropogenic carbon in the Nordic Seas using observed relationships of N, P, and C versus CFCs. *Progress in Oceanography*, *78*(1), 78–84. https://doi.org/10.1016/j.pocean.2007.06.001

Karstensen, J., Schlosser, P., Wallace, D. W. R., Bullister, J. L., & Blindheim, J. (2005). Water mass formation in the Greenland Sea during the 1990s. *Journal of Geophysical Research*, *110*(C7), C07022. https://doi.org/10.1029/2004JC002510

Khatiwala, S., Tanhua, T., Mikaloff Fletcher, S., Gerber, M., Doney, S. C., Graven, H. D., et al. (2013). Global ocean storage of anthropogenic carbon. *Biogeosciences*, *10*(4), 2169–2191. https://doi.org/10.5194/bg-10-2169-2013

Koeve, W., & Kähler, P. (2016). Oxygen utilization rate (OUR) underestimates ocean respiration: A model study. *Global Biogeochemical Cycles*, *30*(8), 1166–1182. https://doi.org/10.1002/2015GB005354

Lauvset, S. K., Brakstad, A., Våge, K., Olsen, A., Jeansson, E., & Mork, K. A. (2018). Continued warming, salinification and oxygenation of the Greenland Sea gyre. *Tellus A: Dynamic Meteorology and Oceanography*, *70*(1), 1–9. https://doi.org/10.1080/16000870.2018.1476434

Lauvset, S. K., Lange, N., Tanhua, T., Bittig, H. C., Olsen, A., Kozyr, A., et al. (2022). GLODAPv2.2022: The latest version of the global interior ocean biogeochemical data product. *Earth System Science Data Discussions*, *2022*, 1–37. https://doi.org/10.5194/essd-2022-293

Macrander, A., Valdimarsson, H., & Jonsson, S. (2014). Improved transport estimate of the East Icelandic Current 2002-2012. *Journal of Geophysical Research: Oceans*, *119*(6), 3407–3424. https://doi.org/10.1002/2013JC009517

Maier-Reimer, E., & Hasselmann, K. (1987). Transport and storage of CO₂ in the ocean—An inorganic ocean-circulation carbon cycle model. *Climate Dynamics*, *2*(2), 63–90. https://doi.org/10.1007/Bf01054491

Marnela, M., Rudels, B., Olsson, K. A., Anderson, L. G., Jeansson, E., Torres, D. J., et al. (2008). Transports of Nordic Seas water masses and excess SF₆ through Fram Strait to the Arctic Ocean. *Progress in Oceanography*, *78*(1), 1–11. https://doi.org/10.1016/j.pocean.2007.06.004

Merbach, C., Culberson, C. H., Hawley, J. E., & Pytkowicz, R. M. (1973). Measurements of the apparent dissociation constants of carbonic acid in seawater at atmospheric pressure. *Limnology & Oceanography*, *18*(6), 897–907. https://doi.org/10.4319/lo.1973.18.6.0897

Messias, M. J., Watson, A. J., Johannessen, T., Oliver, K. I. C., Olsson, K. A., Fogelqvist, E., et al. (2008). The Greenland Sea tracer experiment 1996-2002: Horizontal mixing and transport of Greenland Sea Intermediate Water. *Progress in Oceanography*, *78*(1), 85–105. https://doi.org/10.1016/j.pocean.2007.06.005

Nilsen, J. E. Ø., & Falck, E. (2006). Variations of mixed layer properties in the Norwegian Sea for the period 1948-1999. *Progress in Oceanography*, *70*(1), 58–90. https://doi.org/10.1016/j.pocean.2006.03.014

Nondal, G., Bellerby, R. G. J., Olsen, A., Johannessen, T., & Ólafsson, J. (2009). Optimal evaluation of the surface ocean CO₂ system in the northern North Atlantic using data from voluntary observing ships. *Limnology and Oceanography: Methods*, *7*(1), 109–118. https://doi.org/10.4319/lom.2009.7.109

Ólafsson, J. (2003). Winter mixed layer nutrients in the Irminger and Iceland Seas, 1990-2000. *ICES Marine Science Symposia*, *219*, 329–332.

Ólafsson, J., Smethie, W. M., Jr., Ólafsdóttir, S. R., Danielsen, M., & Sveinbjörnsdóttir, Á. E. (2023). Biogeochemistry, transient tracers and oxygen isotopes from discrete samples and profile observations during the R/Vs Arni Fridriksson and the Bjarni Saemundsson seasonal cruises in the North Atlantic Ocean from 2002-02-15 to 2006-05-29 (NCEI Accession 0276771). [Dataset]. NOAA National Centers for Environmental Information. Unpublished Dataset https://ncei.noaa.gov/archive/accession/0276771

Olsen, A., Lange, N., Key, R. M., Tanhua, T., Alvarez, M., Becker, S., et al. (2019). GLODAPv2.2019—An update of GLODAPv2. *Earth System Science Data*, *11*(3), 1437–1461. https://doi.org/10.5194/essd-11-1437-2019

Olsen, A., Omar, A. M., Jeansson, E., Anderson, L. G., & Bellerby, R. G. J. (2010). Nordic Seas transit-time distributions and anthropogenic CO_2. *Journal of Geophysical Research*, *115*(C5), C05005. https://doi.org/10.1029/2009JC005488

Olsen, A., Omar, A. M., Bellerby, R. G. J., Johannessen, T., Ninnemann, U., Brown, K. R., et al. (2006). Magnitude and origin of the anthropogenic CO_2 increase and ^{13}C Suess effect in the Nordic Seas since 1981. *Global Biogeochemical Cycles*, *20*(3), GB3027. https://doi.org/10.1029/2005GB002669

Olsson, K. A., Jeansson, E., Tanhua, T., & Gascard, J.-C. (2005). The East Greenland Current studied with CFCs and released sulphur hexafluoride. *Journal of Marine Systems*, *55*(1–2), 77–95. https://doi.org/10.1016/j.jmarsys.2004.07.019

Østerhus, S., & Gammelsrød, T. (1999). The abyss of the Nordic Seas is warming. *Journal of Climate*, *12*(11), 3297–3304. https://doi.org/10.1175/1520-0442(1999)012<3297:Taotns>2.0.Co;2

Poulain, P. M., Warn-Varnas, A., & Niiler, P. P. (1996). Near-surface circulation of the Nordic Seas as measured by Lagrangian drifters. *Journal of Geophysical Research*, *101*(C8), 18237–18258. https://doi.org/10.1029/96JC00506

Raimondi, L., Tanhua, T., Azetsu-Scott, K., Yashayaev, I., & Wallace, D. W. R. (2021). A 30-year time series of transient tracer-based estimates of anthropogenic carbon in the central Labrador Sea. *Journal of Geophysical Research: Oceans*, *126*(5), e2020JC017092. https://doi.org/10.1029/2020JC017092

Rajasakaren, B., Jeansson, E., Olsen, A., Tanhua, T., Johannessen, T., & Smethie, W. M. (2019). Trends in anthropogenic carbon in the Arctic Ocean. *Progress in Oceanography*, *178*, 102177. https://doi.org/10.1016/j.pocean.2019.102177

Rhein, M. (1991). Ventilation rates of the Greenland and Norwegian Seas derived from distributions of the chlorofluoromethanes F11 and F12. *Deep-Sea Research, Part A: Oceanographic Research Papers*, *38*(4), 485–503. https://doi.org/10.1016/0198-0149(91)90048-K

Ronski, S., & Budéus, G. (2005). Time series of winter convection in the Greenland Sea. *Journal of Geophysical Research*, *110*(C4), C04015. https://doi.org/10.1029/2004JC002318

Rudels, B., Björk, G., Nilsson, J., Winsor, P., Lake, I., & Nohr, C. (2005). The interaction between waters from the Arctic Ocean and the Nordic Seas north of Fram Strait and along the East Greenland Current: Results from the Arctic Ocean-02 Oden expedition. *Journal of Marine Systems*, *55*(1–2), 1–30. https://doi.org/10.1016/j.jmarsys.2004.06.008

Rudels, B., Friedrich, H. J., & Quadfasel, D. (1999). The Arctic circumpolar boundary current. *Deep-Sea Research II*, *46*(6–7), 1023–1062. https://doi.org/10.1016/S0967-0645(99)00015-6

Sabine, C. L., Feely, R. A., Gruber, N., Key, R. M., Lee, K., Bullister, J. L., et al. (2004). The oceanic sink for anthropogenic CO_2. *Science*, *305*(5682), 367–371. https://doi.org/10.1126/science.1097403

Sabine, C. L., & Tanhua, T. (2010). Estimation of anthropogenic CO_2 inventories in the ocean. *Annual Reviews of Marine Science*, *2*(1), 269–92. https://doi.org/10.1146/annurev-marine-120308-080947

Schlosser, P., Bönisch, G., Rhein, M., & Bayer, R. (1991). Reduction of deepwater formation in the Greenland Sea during the 1980s: Evidence from tracer data. *Science*, *251*(4997), 1054–1056. https://doi.org/10.1126/science.251.4997.1054

Shao, A. E., Mecking, S., Thompson, L., & Sonnerup, R. E. (2013). Mixed layer saturations of CFC-11, CFC-12, and SF_6 in a global isopycnal model. *Journal of Geophysical Research: Oceans*, *118*(10), 4978–4988. https://doi.org/10.1002/jgrc.20370

Shao, A. E., Mecking, S., Thompson, L., & Sonnerup, R. E. (2016). Evaluating the use of 1-D transit time distributions to infer the mean state and variability of oceanic ventilation. *Journal of Geophysical Research: Oceans*, *121*(9), 6650–6670. https://doi.org/10.1002/2016JC011900

Shao, Q., Zhao, J., Drinkwater, K. F., Wang, X., & Cao, Y. (2019). Internal overflow in the Nordic Seas and the cold reservoir in the northern Norwegian Basin. *Deep Sea Research Part I: Oceanographic Research Papers*, *148*, 67–79. https://doi.org/10.1016/j.dsr.2019.04.012

Smith, J. N., Smethie, W. M., Jr., & Casacuberta, N. (2022). Synoptic ^{126}I and CFC-SF_6 transient time distribution (TTD) sections across the central Arctic Ocean from the 2015 GEOTRACES cruises. *Journal of Geophysical Research: Oceans*, *127*(9), e2021JC018120. https://doi.org/10.1029/2021JC018120

Somavilla, R., Schauer, U., & Budéus, G. (2013). Increasing amount of Arctic Ocean deep waters in the Greenland Sea. *Geophysical Research Letters*, *40*(16), 4361–4366. https://doi.org/10.1002/grl.50775

Sonnerup, R. E., Bullister, J. L., & Warner, M. J. (2008). Improved estimates of ventilation rate changes and CO_2 uptake in the Pacific Ocean using chlorofluorocarbons and sulfur hexafluoride. *Journal of Geophysical Research*, *113*(C12), C12007. https://doi.org/10.1029/2008JC004864

Stöven, T., & Tanhua, T. (2014). Ventilation of the Mediterranean Sea constrained by multiple transient tracer measurements. *Ocean Science*, *10*(3), 439–457. https://doi.org/10.5194/os-10-439-2014

Stöven, T., Tanhua, T., Hoppema, M., & Bullister, J. L. (2015). Perspectives of transient tracer applications and limiting cases. *Ocean Science*, *11*(5), 699–718. https://doi.org/10.5194/os-11-699-2015

Stöven, T., Tanhua, T., Hoppema, M., & von Appen, W. J. (2016). Transient tracer distributions in the Fram Strait in 2012 and inferred anthropogenic carbon content and transport. *Ocean Science*, *12*(1), 319–333. https://doi.org/10.5194/os-12-319-2016

Swift, J. H. (1986). The Arctic waters. In B. G. Hurdle (Ed.), *The Nordic Seas* (pp. 129–153). Springer-Verlag.

Swift, J. H., & Aagaard, K. (1981). Seasonal transitions and water mass formation in the Iceland and Greenland Seas. *Deep-Sea Research, Part A: Oceanographic Research Papers*, *28A*(10), 1107–1129. https://doi.org/10.1016/0198-0149(81)90050-9

Talley, L. D., Pickard, G. L., Emery, W. J., & Swift, J. H. (2011). *Descriptive physical oceanography: An introduction* (6th ed., p. 560). Elsevier.

Tanhua, T., Bulsiewicz, K., & Rhein, M. (2005). Spreading of overflow water from the Greenland to the Labrador Sea. *Geophysical Research Letters*, *32*(10), L10606. https://doi.org/10.1029/2005gl022700

Tanhua, T., Olsson, K. A., & Jeansson, E. (2005). Formation of Denmark Strait overflow water and its hydro-chemical composition. *Journal of Marine Systems*, *57*(3–4), 264–288. https://doi.org/10.1016/j.jmarsys.2005.05.003

Tanhua, T., Waugh, D. W., & Wallace, D. W. R. (2008). Use of SF_6 to estimate anthropogenic CO_2 in the upper ocean. *Journal of Geophysical Research*, *113*(C4), C04037. https://doi.org/10.1029/2007JC004416

Thomas, H., & England, M. (2002). Different oceanic features of anthropogenic CO_2 and CFCs. *Naturwissenschaften*, *89*(9), 399–403. https://doi.org/10.1007/s00114-002-0348-5

Thomas, J. L., Waugh, D. W., & Gnanadesikan, A. (2020). Relationship between age and oxygen along line W in the northwest Atlantic Ocean. *Ocean Science Journal*, *55*(2), 203–217. https://doi.org/10.1007/s12601-020-0019-5

Våge, K., Moore, G. W. K., Jónsson, S., & Valdimarsson, H. (2015). Water mass transformation in the Iceland Sea. *Deep Sea Research Part I: Oceanographic Research Papers*, *101*(0), 98–109. https://doi.org/10.1016/j.dsr.2015.04.001

Walker, S. J., Weiss, R. F., & Salameh, P. K. (2000). Reconstructed histories of the annual mean atmospheric mole fractions for the halocarbons CFC-11, CFC-12, CFC-113 and carbon tetrachloride. *Journal of Geophysical Research C: Oceans*, *105*(C6), 14285–14296. https://doi.org/10.1029/1999JC900273

Wallace, D. W. R., & Lazier, J. R. N. (1988). Anthropogenic chlorofluoromethanes in newly formed Labrador Sea Water. *Nature*, *332*(6159), 61–63. https://doi.org/10.1038/332061a0

Warner, M. J., & Weiss, R. F. (1985). Solubilities of chlorofluorocarbons 11 and 12 in water and sea water. *Deep-Sea Research*, *32*(12), 1485–1497. https://doi.org/10.1016/0198-0149(85)90099-8

Watson, A. J., Messias, M. J., Fogelqvist, E., Van Scoy, K. A., Johannessen, T., Oliver, K. I. C., et al. (1999). Mixing and convection in the Greenland Sea from a tracer-release experiment. *Nature*, *401* (6756), 902–904. https://doi.org/10.1038/44807

Waugh, D. W., Haine, T. W. N., & Hall, T. M. (2004). Transport times and anthropogenic carbon in the subpolar North Atlantic Ocean. *Deep-Sea Research I*, *51*(11), 1475–1491. https://doi.org/10.1016/j.dsr.2004.06.011

Waugh, D. W., Hall, M. H., & Haine, T. W. N. (2003). Relationships among tracer ages. *Journal of Geophysical Research C: Oceans*, *108*(C5), 3138. https://doi.org/10.1029/2002JC001325

Waugh, D. W., Hall, T. M., McNeil, B. I., Key, R., & Matear, R. J. (2006). Anthropogenic CO_2 in the oceans estimated using transit time distributions. *Tellus*, *58B*, 376–389. https://doi.org/10.1111/j.1600-0889.2006.00222.x

References From the Supporting Information

Swift, J. H., & Koltermann, K. P. (1988). The origin of Norwegian Sea Deep Water. *Journal of Geophysical Research*, *93*(C4), 3563–3569. https://doi.org/10.1029/JC093iC04p03563